ESTIMATION OF SEISMIC VELOCITY USING SURFACE WAVE DISPERSION

A DISSERTATION

Submitted in partial fulfillment of the

Requirement for the award of the degree

Of

MASTER OF TECHNOLOGY

In

GEOPHYSICAL TECHNOLOGY

By

NARESH KUMAR

DEPARTMENT OF EARTH SCIENCES
INDIAN INSTITUTE OF TECHNOLOGY ROORKEE
ROORKEE -247667 (INDIA)
MAY 2016

CANDIDATE DECLARATION

I hereby declare that the work presented in this dissertation entitled "**ESTIMATION OF SEISMIC VELOCITY USING SURFACE WAVE DISPERSION**" is in partial fulfillment of the requirements for the award of the degree of Integrated Master of Technology in Geophysical Technology and submitted to the Department of Earth Sciences, Indian Institute of Technology Roorkee is an authentic record of my own dissertation work carried out during the period from June 2015 to May 2016, under the kind supervision of **Dr. Sagarika Mukhopadhyay**, Professor, Department of Earth Sciences, Indian Institute of Technology Roorkee. The matter presented in this dissertation has not been submitted by me for the award of any other degree of this or any other institute.

DATE: **(NARESH KUMAR)**

PLACE: ROORKEE M.tech Geophysical Technology

DEAPARTMENT OF EARTH SCIENCES

IIT ROORKEE

ROORKEE-247667, INDIA

CERTIFICATE

This is to certify that the above statements made by the candidate are correct to the best of my knowledge.

(Prof. Sagarika mukhopadhyay)

Professor

DEAPARTMENT OF EARTH SCIENCES

IIT ROORKEE

ROORKEE-247667, INDIA

ACKNOWLEDGEMENT

I first and foremost would like to express my sincere gratitude to my guide ***Professor Sagarika Mukhopadhyay*** *for supervising my dissertation work. I am highly indebted to her for her guidance, attention and encouragement which she always offered me throughout my work. I highly appreciate her humble behavior and thank her for all the help & support.*

I am thankful to ***Mr.Amit Kumar*** *with whom I collaborated during this work. I also wish to thank my friends who helped me during my work. Finally, I thank my family for their help and support.*

Naresh Kumar

ABSTRACT

In this research work an attempt has been made to observe the variation in dispersion curves characteristic of the surface waves using broadband data in all the direction around Bhopal station. The seismic events chosen are within the regional distance, shallow focused and with magnitude greater than 5 Mb. These earthquakes are located in all the direction around Bhopal station. Since dispersion curves give the average value along its ray path, our investigation focusses on finding the seismic velocity in all the direction and then comparing with each other.

Multiple filter technique is applied to compute the group velocities of the surface waves from the dispersion curves. The measured dispersion curves for this data set are within the period of 10-100 sec for all the 9 cluster around Bhopal station.

Group velocity is further computed using the weighted average and higher order polynomial fir to estimate trend of trajectory between station and epicenters of the earthquakes. It is observed that Love and Rayleigh group velocities are highest reaching 4.5km/sec for love wave in the cluster 9 in which events are present in bay of Bengal. Also in other clusters, in cluster no. 2 the group velocity of both love and Rayleigh wave exceed the 4km/sec. In cluster 4,5 and 6 difference between Love and Rayleigh wave group velocities are higher at smaller period. Whereas difference is less at higher period. But in cluster 9 and 10 difference between Love and Rayleigh wave group velocities are higher at larger period whereas difference is less at smaller period.

On the basis of number of available dispersion curves at higher period, selected period range for inversion lies in between 10-95 sec. The inversion process is approached by combining the Love and Rayleigh group velocities. The depth up to 180 km can be resolved. As usual we found the moho at 12-15km for the oceanic crust for the cluster no.9 and in continental region moho is at highest depth of approx. 65km for cluster 4 which is slightly west of the north from Bhopal station or we can say hind-kush region. The depth up to 180 km can be resolved. The observed high-velocity for cluster 9 is explained by a higher density oceanic crust.

CONTENT

LIST OF FIGURES

LIST OF TABLES

CHAPTER#1 INTRODUCTION

1.1.Brief Preview

Frequency of seismic activities are very high in Indian sub-continent. Northern boundary of Indian plate is going under Eurasian plate so this region is seismically very active.
In east Indian plate is obliquely converging with Burma plate (Fitch, 1972; Curray et al., 1979). In west Indian and Arabian plate are seprated by Owen Fracture Zone (OFZ) and both plate are moving towards north at a differential rate (Fournier M., 2011). In south west indian plate is interacting with sunda and Australian plate. So the region around Indian has shown lot of earthquake of magnitude greater than 5. To compare the group velocity in all the direction around Indian sub-continent surface velocity are studied. So the difference in are assigned to the crustal composition and tectonic activities confronted in the wave path. First Dziewnoski (1969) made the multiple filter technique. Then it is modified by Hermann (2007). To obtain better results we used this technique and also weighted average polynomial fit is used.

1.2.Objective

To study the dispersion curves for the events starting from all the direction around Indian sub-continent and differentiate their values at station BHOPAL.

Compare the group velocity for Rayleigh and Love wave in all the directions. To find out the is there is any change in parameters in all the direction and make an effort to analyze it in terms of tectonic environment in all the direction around Indian plate.

To find the S-wave velocity structure through inversion of dispersion curves.

From above study I would like evaluate the originative factor of the difference in velocity in all the directions.

CHAPTER#2 GEOLOGY AND TECTONICS OF STUDY AREA

2.1. Tectonic feature of INDIAN PLATE

The Indian plate is surrounded by active deformation zones. Indian plate is still under thrusting the Eurasian plate. From the the northern edge of India plate along the Himalaya deformation extends from Tibet and into China, up to Russia. In east, Indian plate is subducting under Burma plate in the Andaman-Nicobar Islands region. In the south there is no distinct boundary between the India plate and the Australian plate.

In west direction Indian plate is separated from from the Somalian and Arabian plates by the Central Indian Ridge, the Carlsberg Ridge and Owen Fracture zone respectively.

Indian plate is converging towards Asian plate at a rate of 54 mm/yr (0.054 m/yr) (De Mets et al., 1994). Inside the indian plate there are many tectonic feature like Himalayan mountain belt, Sindhu-Ganga-Brahmaputra alluvial plains, Sindhu-Ganga-Brahmaputra alluvial plains.

2.2. Indian Intraplate Deformation

The Indian shield is made up of different complex rift zones and several thrust. Indian shield is putted into category of Stable Continental Region (SCR). Though , Indian shield has witnessed many earthquakes of magnitude six or more from 18th Century, (Bhatia et al., 1999). The most significant tectonic features of the Indian shield is Narmada-Son Lineament (NSL) which divides the shield into northern and southern sectors (Bhatia et al., 1999). In last forty years 285 earthquakes have occurred having different magnitude and varied focal depths (Khan, 2009).

Tectonics of of the northeastern part of India is very complex due to active north-south convergence along the Himalaya (Seeber et al., 1981). In the Northeast India due to Shillong plateau north-south shortening is occurring, this cause great (MW 8.1) Assam earthquake of 1897.

2.3 Indian Inter-plate Deformation

Figure2.1 shows the boundaries of neighboring plates with Indian plate. Where figure 2.2 shows the type of interaction of neighboring plates with Indian tectonic plate which are divided into seven classes by Peter Bird (2003).

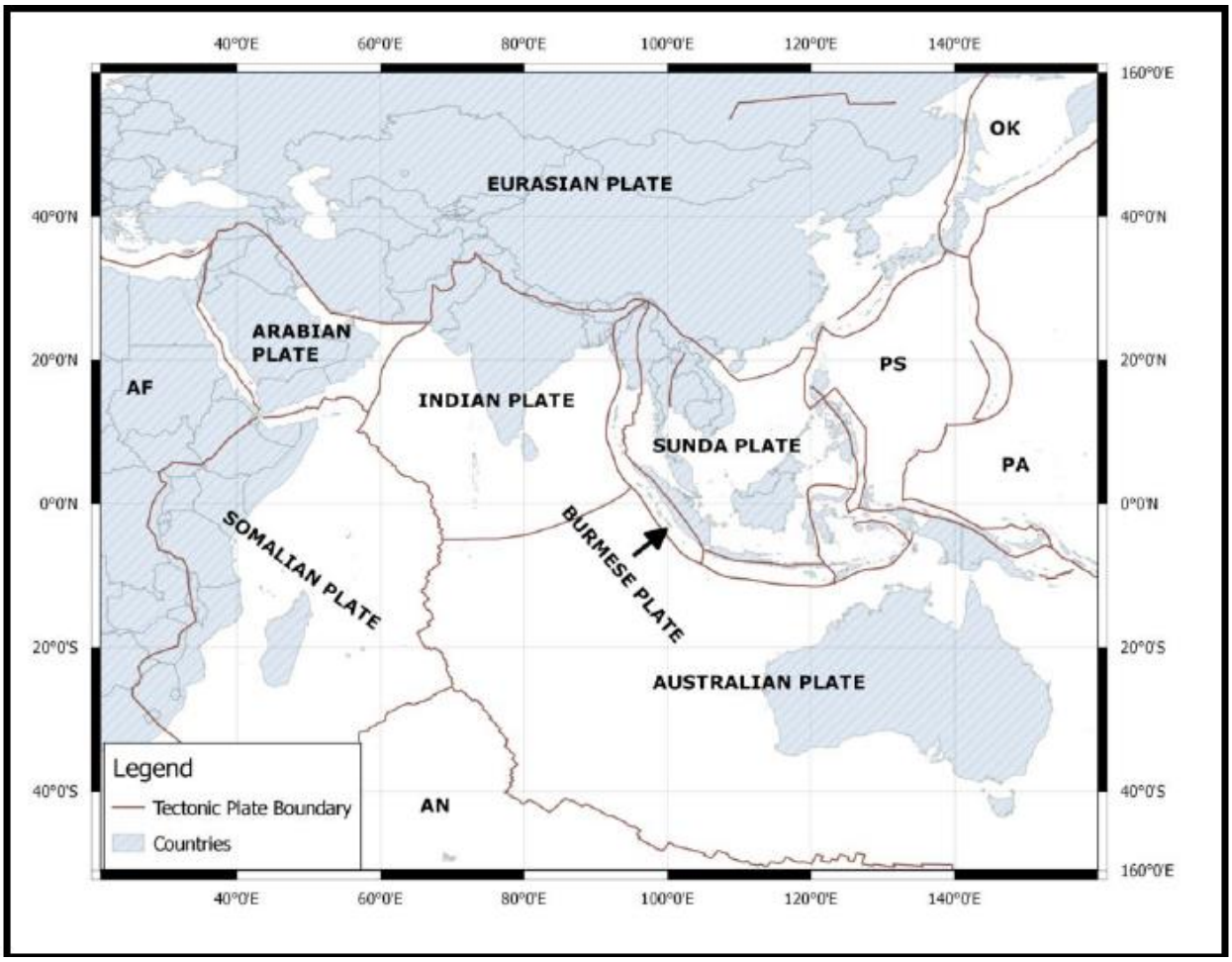

Figure2.1 Indian Tectonic Plate with Its Neighbouring Plates

(Data: Peter Bird, 2003)

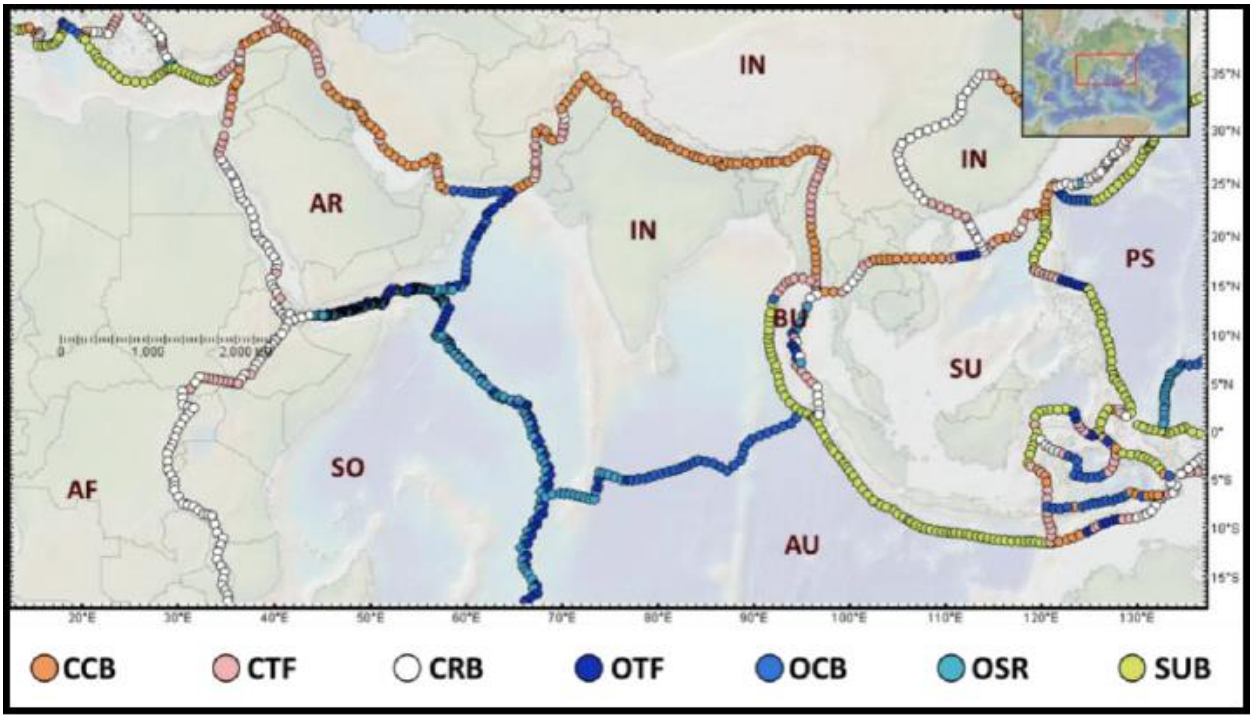

Figure 2.2: Indian Tectonic Plate with Its Neighboring Plates and Interaction Types (Data: Peter Bird, 2003**)**

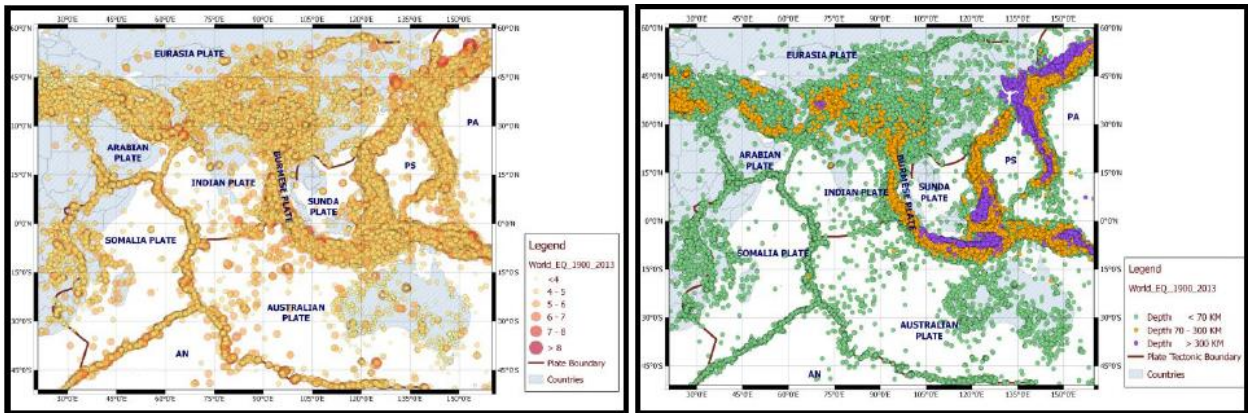

(a) **(b)**

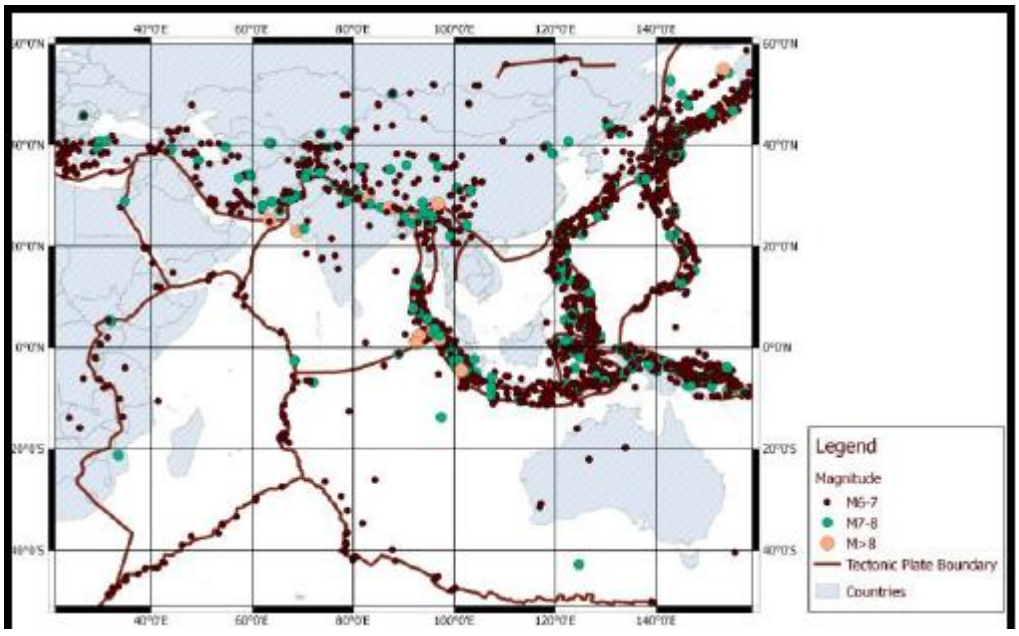

(c)

Figure 2.3: Epicenters in and around Indian Tectonic Plate (a) Figure Shows Epicenters with Different Magnitudes (b) Figure Shows Epicenters with Different Depths (c) Figure Shows Epicenters of Earthquakes Whose Magnitude is Equal or Greater than 6 (Earthquake Data: NCEDC)

CHAPTER#3 THEORY OF SURFACE WAVE

3.1. Surface waves

Surface waves are defined as those produced in media with free surface which propagate parallel to the surface and whose amplitudes decrease with the distance from surface. Surface waves are generated by energy brought to the free surface by incident waves. Their existence is related to the presence of free surface. Although they are affected by other surfaces of contact between layers of different elastic properties. Surface waves are generated by constructive interference of body waves in connection with free surface (Shearer, 2009).

Surface waves are of two kinds namely Love waves and Rayleigh waves (Figure 3.1).

Love waves

Love waves are formed through the constructive interference of high-order SH surface multiples (i.e., SSS, SSSS, SSSSS, etc.). Thus, it is possible to model Love waves as a sum of body waves

Rayleigh Waves

For SH polarized waves, the reflection coefficient at the free surface is one, and the interference between the downgoing SH waves and those turned back toward the surface produces Love waves. The P/SV system is more complicated because the surface reflections involve both P and SV waves. In this case, the upgoing and downgoing body waves do not sum constructively to produce surface waves. However, a solution is possible for inhomogeneous waves trapped at the interface; the resulting surface waves are termed Rayleigh waves. (Shearer, 2009).

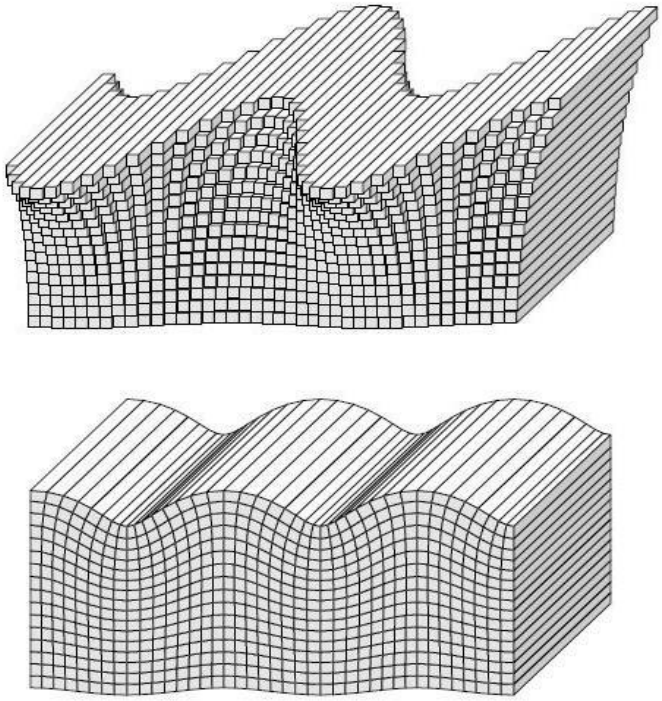

Figure 3.1. Fundamental Love (top) and Rayleigh (bottom) surface wave displacements (highly exaggerated) for horizontal propagation across the page. Love waves are purely transverse motion, whereas Rayleigh waves contain both vertical and radial motion. In both cases, the wave amplitude decays strongly with depth.(after Shearer, 2009)

3.2. Dispersion

When different frequency components travel at different phase velocities, pulse shapes will not stay the same as they travel but will become dispersed as the frequencies separate. This leads to interference effects that cancel the wave energy except at particular times defined by the group velocity of the wave. This may be illustrated by considering the sum of two harmonic waves of slightly different frequency and wavenumber (Shearer, 2009):

$u(x, t) = \cos(\omega 1t - k1x) + \cos(\omega 2t - k2x).$ (3.1)

Relative to an average frequency ω and wavenumber k, we have

$\omega 1 = \omega - \delta\omega, k1 = k - \delta k,$ (3.2

$\omega 2 = \omega + \delta\omega, k2 = k + \delta k.$ (3.3)

Substituting into (3.1), we obtain

$u(x, t) = \cos(\omega t - \delta\omega t - kx + \delta kx) + \cos(\omega t + \delta\omega t - kx - \delta kx)$

$= \cos [(\omega t - kx) - (\delta\omega t - \delta kx)] + \cos [(\omega t - kx) + (\delta\omega t - \delta kx)]$

$= 2 \cos(\omega t - kx) \cos(\delta kx - \delta\omega t),$ (3.4)

where we have used the identity 2 cos*A*cos*B* = cos*(A + B)* + cos*(A − B)*. The resulting waveform consists of a signal with the average frequency ω whose amplitude is *modulated* by a longer period wave of frequency $\delta\omega$.

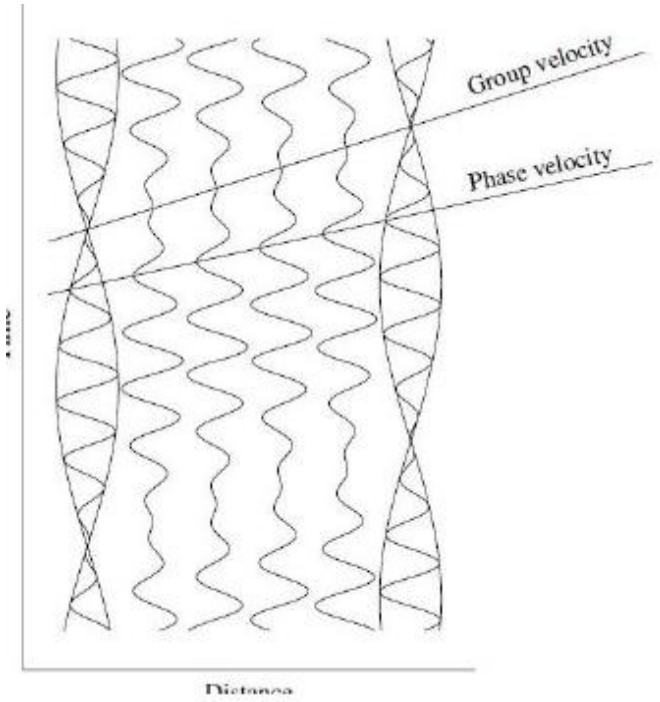

Figure 3.2. The sum of two waves of slightly different frequencies results in a modulated wave. The group velocity is the velocity of the wave packets; the phase velocity is the velocity of the individual peaks. (Shearer, 2009).

In acoustics, this phenomenon is termed beating and may be observed when two musical notes are slightly out of tune. The short-period wave travels at velocity ω/k and the longer period envelope travels at velocity δω/δk. The former is the phase velocity c; the latter is the group velocity U. In the limit as δω and δk approach zero, we thus have

U = dω/dk (3.5) which agrees with our previous result. Using the various relationships between the harmonic wave parameters the group velocity may be alternatively expressed as

U = dω/dk

= c + kdc/dk

= c(1 – kdc/dω)−1

For Earth, the phase velocity c of both Love and Rayleigh waves generally increases with period; thus $dc/d\omega$ is negative and from equation it follows that the group velocity is less than the phase velocity ($U < c$).

Figure 3.3. Plots Love and Rayleigh dispersion curves computed from the PREM model. A minimum or maximum point on the group velocity dispersion curve will result in energy from a range of periods arriving at nearly the same time. This is termed an Airy phase and occurs in Earth for Rayleigh waves at periods of about 50 and 240 s.

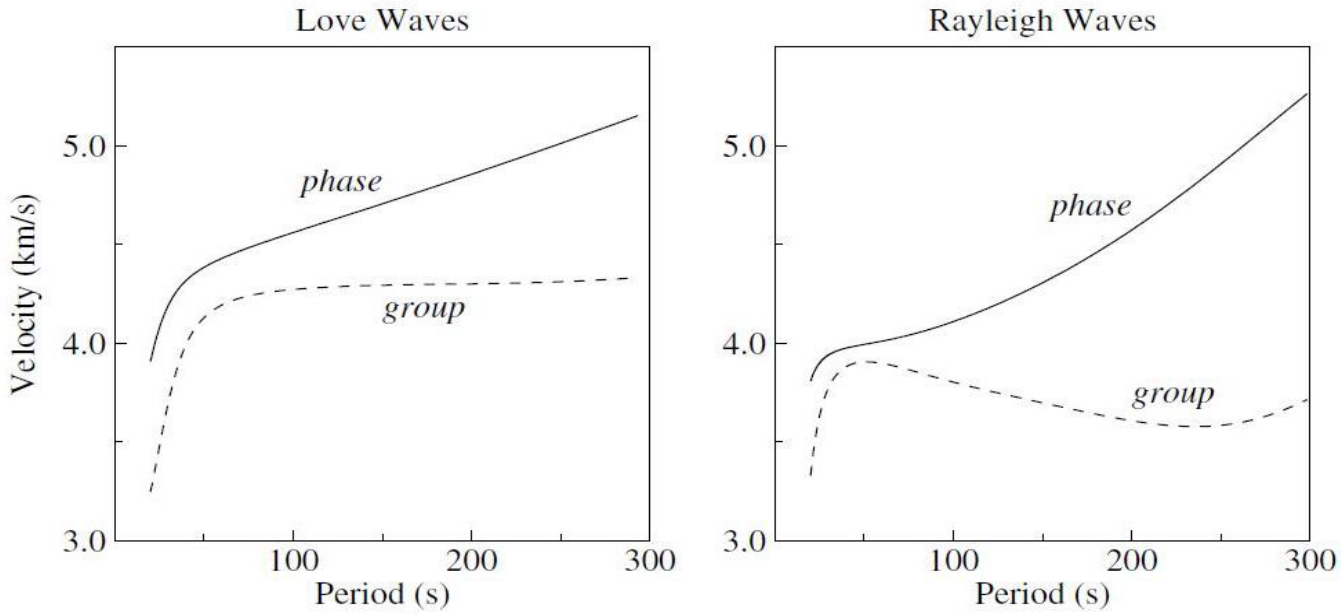

Figure 3.3. Fundamental Love and Rayleigh dispersion curves computed from the isotropic PREM model (after Shearer, 2009).

3.3. Group Velocity

The group velocity can be determined from the record of surface waves at a single station. If we correct for the instrument phase shift Ø1, the phase is given by

$$\varphi = kx - \omega t + \emptyset \pm \pi/4$$

On taking the derivative with respect to ω and, since $d\omega/dk = U$, solving for U, we obtain

$$U = \frac{x}{\frac{d\emptyset}{d\omega} + \frac{d\varphi}{d\omega} + t}$$

For a stationary phase $/d\omega = 0$ and $\omega = \omega 0$. Assuming that initial phase doesn't depend on frequency. We obtain for each instantaneous frequency $\omega 0$.

$$(\omega 0) = x/(\omega 0)$$

The method for determination of the group velocity consist in measuring times of arrival of peak and trough of waves in a disperse train (these are phases $\varphi = 0$ and π.(Figure 3.4(a)) These values are represented in a plot with respect to the order number (Figure 3.4(b)). On doubling the intervals between pairs of values (or from peak to peak) we obtain the periods corresponding to instantaneous frequency and, from the ordinates, we obtain their arrival times. On dividing the epicentral distance by each arrival time, we obtain the group velocity ($T0$) for each period (Figure 3.4. (c)). This velocity corresponds to mean of the structure along the trajectory from the epicenter to the station.

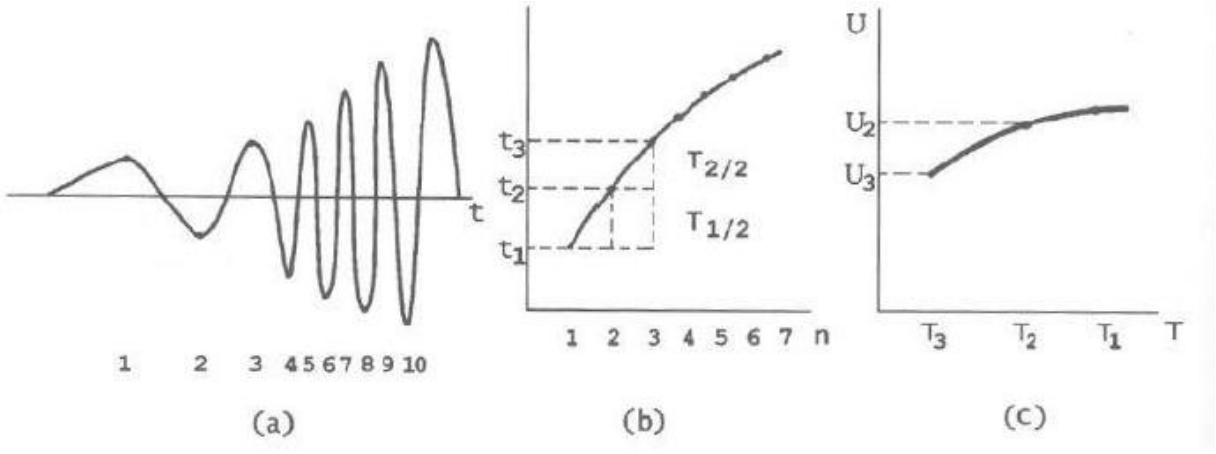

Figure 3.4. Determination of the group velocity from the instantaneous frequencies at one station. (a) Identification of peaks and troughs, (b) Travelling times of peaks and troughs and determination of their periods. (c) The group velocities corresponding to each period (Udias, 1999).

CHAPTER #4 THEORY OF MULTIPLE FILTER ANALYSIS

4.1. Multiple filter Analysis

The multiple filter technique is shown to be a fast, efficient method of analyzing multiply dispersed signals. The amplitudes and a phases of signals passed by an array of narrow band filters can be used to measure group velocity as a function of period and velocity, lateral refraction, modal vibrations of the surface, and other dispersion parameters associated with variety of modes recorded by a single station for one event.

This technique can recover broader portions of the dispersion present in ordinary recording, compared to classical peak and trough method. Thus this technique often shows greater frequency resolution, when compared with those calculated by moving window process (Dzienwnoski, 1969). The method resolves complex transient signals composed of several dominant periods that arrive at recording station almost simultaneously. Instantaneous spectral amplitude, presented in dB as a function of period and group velocity may be interpreted in terms of multi-mode group velocity. When mutually orthogonal components of the motions are analyzed, the results can be used to study the three dimensional vibration of the recording site in terms of the ellipticity and phase for each of the observed propagating modes.

In practice the filtration is done is frequency domain as it has definite advantages over its time domain equivalent. Firstly it is possible to use filter functions whose inverse transforms cannot be expressed in terms of elementary functions. Also its fast as FFT is faster than convolutions in time domain.

The MFT is used to study variations of amplitude (or energy) of a signal as a function of velocity (time) and period (frequency). It is hence required to have a filtering function with good resolutions in immediate vicinity of each center frequency and velocity value. Thus Gaussian function was chosen as it meet these requirement.

A system of filters with constant Q is appropriate for the analysis of most dispersed signal, since this leads to constant resolution on log-period scale. If ωn denotes the centre frequency for the nth column, the window function can be written

$$H(\omega) = e^{-\alpha(\frac{\omega-\omega_n}{\omega_n})^2}$$

The Fourier transform of (ω) is

$$h_n(t) = \frac{\sqrt{\pi}.w_n}{2\alpha}.e^{\frac{\omega_n^n.t^2}{4\alpha}}.\mathrm{Cos}(\omega_n t)$$

The resolution is controlled by parameter α. Levshin (1989) recommends associating the instantaneous frequency with the group arrival time, but this is not always effective. One could use the group times associated with two filter parameters α as developed by Hermann (2002), but the difficulty of automatically associating the corresponding envelope peaks for different α's is not trivial. The spectral amplitude estimate is good only when the is larger as distance increases. The following choices of α may be adequate for the period range of 4 - 100 sec:

Distance Range (km)	α
1000	25
2000	50
4000	100
8000	200

CHAPTER#5 THEORY OF INVERSION

5.1. Introduction

In physical science, obtaining information about physical parameters from data is an important aspect. Physical laws provides general means to obtain the values from a mode. This is known as 'Forward problem'. Inverse problem aims to recreate a set of measurement from the data. Ideally the background theory drives the data to be transformed so as to construct a model. The above concept can easily be understood with the help Figure 5.1. (Snieder, 2003).

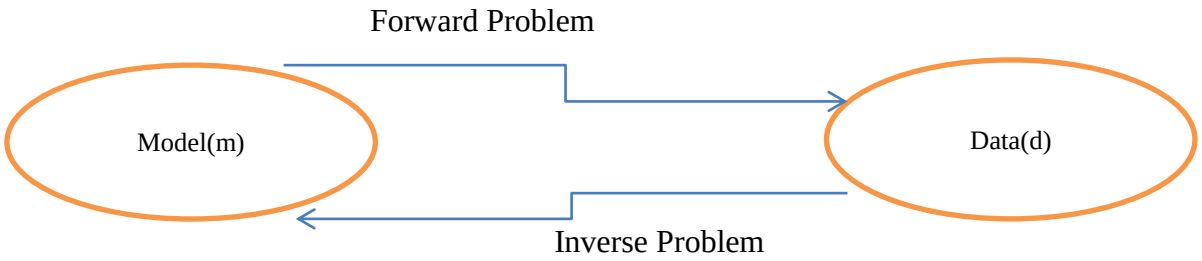

Figure 5.1. Forward problems and inverse problems representation

Even though Inversion possess mathematical elegance still the exact nonlinear inversion schemes are of limited usage. The reasons being many. First of all the inversion technique to obtain exact results are applicable only to ideal cases which hold no practical significance. Secondly the exact inversion methods are quite unstable. The third reason is most fundamental one. In inverse problems the obtained model aspires to be a continuous function of space variables. Thus making the degree of freedom to be infinite. In reality the amount of data used is finite. Thus making the count of variables shows the data information required to obtain the model uniquely is insufficient.

Hence in reality one tries to obtain a model with infinite degree of freedom from a data of limited information thus making the solution a non-unique one. Hence the model obtained from data need not represent the true model. Thus the inverse problem represented in the flow chart above is notthat simple. For realistic problems, inversion is carried in two steps. First we define a true model denoted by m from data denoted by d. From d we obtain an estimated model $\acute{m}$, known as estimation problem. (Figure 5.2)

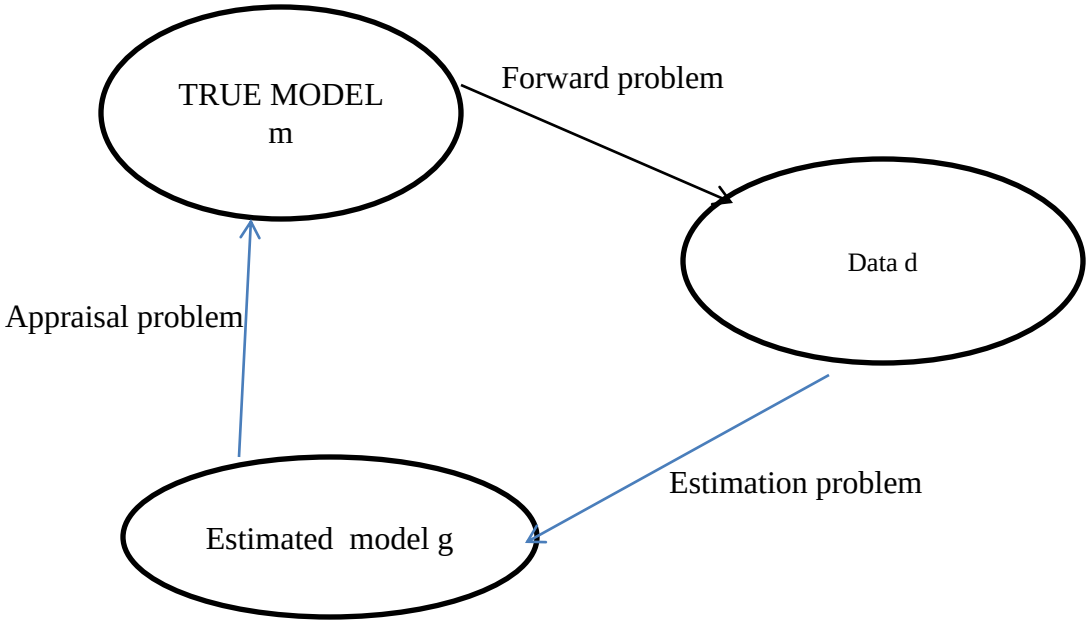

Figure 5.2. Inverse problem as a combination of estimation problem and appraisal problem

Apart from obtaining the estimated model m' its relation with true model m must be established. An appraisal problem is constituted which will give information on obtaining the properties of true model m which can be determined from the estimated model m' and amount of error associated with it. In short it can be summed as Inversion=estimation + appraisal. Thus it makes more sense to obtain a physical interpretation of a model by acknowledging the amount of error and limit of resolution of model (Trampert, 1998)

Thus in order to proceed further with steps of inversion a review of basic concept of regression analysis.

5.2. Means, Variances and Standard Deviations

Let xi be the i'th measured distance. Let N be the number of times the experiment is repeated. Let the expected value of x, E(x), be m, which we call the mean. Finally let ei be the random error of the i'th observation. Thus the i'th observation is

$$x_i = m + e_i$$

At this point an important assumption is made about the random error process – this process has a zero mean, i.e., E(e) = 0. This can be written as

$$\frac{1}{N}\sum_{i=1}^{N} \epsilon_i \rightarrow 0$$

That there is no bias in the measurements, as might arise from a bad measuring scale, is an article of faith. Further we assume that the errors are truly random and not correlated. Although not necessary here, the error is often assumed to arise from a normal, or Gaussian, distribution with zero mean and variances σ.

For such a distribution, we expect about 68% of the observations to lie within the range $(\mu - \sigma, \mu + \sigma)$, and 95% within the range $(\mu - 2\sigma, \mu + 2\sigma)$

Mathematically the normal distribution N(z, σ2) is defined as

$$N(z,\sigma^2) = \frac{1}{\sigma\sqrt{2\pi}} e^{-z^2 6/2\sigma^2}$$

This is a probability distribution and the $\int_{-\infty}^{z} N(z,\sigma^2)dz$ is called the cumulative probability, which varies from 0 at Z = -∞ to 1 at Z = +∞

Our task is to use all observations to estimate the μ and the variance σ2. We acknowledge that we cannot determine the m, but only estimate an x since we have only a finite number of observations. One way to accomplish this is by trying to find an a that minimizes the sum of square residuals

$$S = \sum_{-1}^{N} (x_{i-a})^2$$

This value is determined by requiring $dS/dx = 0$ Solving gives

$$a = \frac{1}{N}\sum_{i=1}^{N} x_i$$

The standard deviation s, an estimate of , is defined by

$$s^2 = \frac{1}{N-1}\sum_{i=1}^{N} (x_1 - \bar{x})\text{^}2$$

(the N -1 is used instead of N since x has already been specified and only N -1 pieces of independent information are available to estimate σ^2. This also guarantees that E(s^2) = σ^2.

Because we have only a finite set of observations, the x estimate of m is not perfect. We estimate the standard error of the distribution of x by the relation.

$$s_{\tilde{x}}^2 = \frac{s^2}{N} = \frac{1}{N(N-1)} \sum_{i=1}^{N} (x_i - \tilde{x})^2$$

At this stage, we can examine the residuals, xi - x, and test whether we can reject the hypothesis that the random error process is normal. We could also test the inappropriateness of other distributions. The meaning of the estimated values is simple. If we perform the experiment once by collecting N samples, we are able to estimate the true , the error process variances σ^2 and the variance on the mean, s_x^2

If we perform the experiment again by collecting additional samples from the same noise contaminated population, we would expect the new x to lie about the true m with a distribution controlled by s_x^2. The s^2 indicates the spread in future observations, and the s_x^2

X indicates the spread in the x estimates of.

Finally as the number of observations N increases, we expect that $\bar{x} \to \mu$, $s^2 \to \sigma^2$ and $s_\xi \to 0$, in probability.

If the noise process is assumed to be Gaussian (normal) then confidence limits can be placed on the measured quantities.

5.3. Linear Regression

Assume now that the observed data are generated by a true linear process, e.g ,

Y=A+Bx (A.3.1)

The observations are again affected by a zero mean random error:

yi=A+Bxi+ ε i

Our objective is to use the data to estimate the true values A and B as well as some properties of the ε process.

The least squares problem is to find the a and b that minimizes

$$S(a,b) = \sum_{i=1}^{N} \varepsilon_i^2 = \sum_{i=1}^{N} (y_i - a - bx_i)^2$$

where the a and b are estimates of A and B.

The condition that a and b make S a minimum requires $\frac{ds}{da} = 0 and \frac{ds}{db} = 0$ .. These conditions yield two linear equations, the normal equations, in the unknowns a and b:

$$\begin{bmatrix} N & \sum x_i \\ \sum x_i & \sum x_i \end{bmatrix} \begin{bmatrix} a \\ b \end{bmatrix} = \begin{bmatrix} \sum y \\ \sum x_i y_i \end{bmatrix}$$

(for simplicity the summation indices are dropped). The solution of this linear equation is obtained by taking the inverse of the square matrix which leads to

$$\begin{bmatrix} a \\ b \end{bmatrix} = \frac{1}{N\sum x_i^2 - (\sum x_i)^{\wedge}2} \begin{bmatrix} \sum x_i^2 & -\sum x_i \\ -\sum x_i & N \end{bmatrix} \begin{bmatrix} \sum y_i \\ \sum x_i \ y_i \end{bmatrix}$$

We can easily show that the a and b values arising from the normal equations gives

$$s(a,b) = \sum y_i^2 - a\sum y_i - b\sum x_i y_i$$

The estimated variance of the error process is

$$s^2 = \frac{1}{N-2} s(a,b)$$

The confidence limits on a and b are given through the use of the t-distribution:

$$\Delta a = t\left(N-2, 1-\frac{\alpha}{2}\right)\left[s^2 \frac{\sum x_i^2}{N\sum x_i^2 - (\sum x_i)^2}\right]^{\wedge}\left(\frac{1}{2}\right)$$

$$\Delta a = t\left(N-2, 1-\frac{\alpha}{2}\right)\left[s^2 \frac{N}{N\sum x_i^2 - (\sum x_i)^2}\right]^{\wedge}\left(\frac{1}{2}\right)$$

where t(N-2, 1-α /2) is the Student-t distribution for N -2 degrees of freedom and the 1-α /2 confidence level [For 95% confidence, α =0. 05 and t(∞, 0. 975) =1.96]. If these confidence bounds are interpreted in the same sense as for the simple example of section 2, these are the confidence that the true value of a lies within a±a, and similarly the value of b lies within b±b. There is one slight complication, and that is that the error estimates Δa and Δb may be interrelated.

The confidence limits that the predicted regression line y □a □□bx lies near the true line y =A+Bx are

$$\pm t\left(N-2, 1-\frac{\alpha}{2}\right)\left[s^2 \frac{\sum x_i^2 - 2x\sum x_i + Nx^2}{N\sum x_i^2 - (\sum x_i)^2}\right]^{\wedge}\left(\frac{1}{2}\right)$$

$$\pm t\left(N-2, 1-\frac{\alpha}{2}\right)\left[s^2 \frac{\sum (x-\bar{x})^2}{\sum (x_i-\bar{x})^2}\right]^{\wedge}\left(\frac{1}{2}\right)$$

The confidence limits on the distribution of the data (or future data) about the regression line y =a + bx are

$$\pm t\left(N-2,1-\frac{\alpha}{2}\right)[s^2(1+\frac{\sum x_i^2-2x\sum x_i+Nx^2}{N\sum x_i^2-(\sum x_i)^2})]\text{^}(\frac{1}{2})$$

The first equation gives two hyperbolas about the regression line whose asymptotes are y =(a+Δa) +(b+Δb)x and y=(a-Δa)+(b+Δb)x. If the experiment were repeated, there is (1-α /2)100% chance that the resultant regression line will lie within these limits. The second equation indicates where future data may lie. The hyperbolic nature of the error bound is interesting since it indicates that the prediction error increases as one gets away from the centroid (x, y) of the data set; this is to be expected when extrapolating beyond the data set.

The interrelationship of error in a and b can be examined by searching through possible values of A and B, comparing the sum of squared residuals to that of the least squares solution (Draper and Smith, 1966):

$$S(A,B)=s(a,b)(1+\frac{2}{N-2}F(2,N-2,1-\alpha)$$

Rearranging, one would contour the following function of A and B, which is related to the F-statistic

$$\left(\frac{S(A,B)-S(a,b}{S(a,b)}\frac{N-2}{2}\right)=F(2,N-2,1-\alpha)$$

Because our model was linear, the contours in the (A, B) space satisfying this relation will be ellipses. In general the major axis of the elliptical contour may be inclined, indicating some interdependence between the a and b values. In this case, a change in the value of b causes a change in a.

Since Draper and Smith (1966) may be the only ones to define confidence ellipses in this manner, an alternative expression is

$$[A-a,B-b]\begin{bmatrix} N & \sum x_i \\ \sum x_i & \sum x_i^2 \end{bmatrix}\begin{bmatrix} A-a \\ B-b \end{bmatrix}=2s^2F(z,N-2,1-\alpha)$$

CHAPTER#6 DATA SELECTION

Data Selection

The main objective of the study is concentrated on the surface wave part of the seismogram. The region of interest is all around the Indian plate. Thus events from all the direction around Indian plate were chosen. These events were recorded at BHOPAL. Bhopal station lies at centre in Indian continental mass with coordinates 23°15′N 77°25′E with an elevation from MSL of 527m. As an earthquake travels, the higher frequency energy is filtered away and the signals appear to contain more low frequencies. At large distance, recording an earthquake requires a certain minimum magnitude. Since the interest is only on low frequency (15-100s) signals, only events with magnitude greater than Mb >5 are selected. The maximum depth was taken to be 50km. All the events are at regional distance.

Hence with aforementioned conditions only 180 events were extracted from the event catalog of more than 400 events during 2008-2013. The signal was extracted from 2 minutes prior to event and 30 minutes post event so as to acquire complete surface wave information present at regional distance. The seismometers used were broad-band seismometers. The event catalog is presented in Table.6.1. The map of event and station is given in Figure 6.1.

Table 6.1. Events Catalog from 2008-2013 recorded atBhopal station.

Year	Mon	Day	Hr.	Min.	Sec.	Lat.	Long.	Depth	Mag.
2008	6	24	18	26	50.9	39.88	70.21	49	5
2008	6	25	2	53	26.2	1.41	97.19	16	5.5
2008	6	27	13	7	8.2	10.89	91.78	17	5.9
2008	6	28	12	54	46.36	10.85	91.71	15	6.1
2008	8	1	8	32	43.5	32.14	104.61	10	5.9
2008	8	12	21	3	15.9	31.82	104.88	10	5.1
2008	8	18	14	11	5.62	33.63	91.92	10	5.3
2008	8	21	12	24	30.93	25.04	97.70	10	6
2008	8	25	13	21	58.82	30.90	83.52	12	6.7
2008	8	26	23	54	23.7	30.66	83.28	10	5
2008	8	27	1	35	39.6	30.69	83.09	15	5.4
2008	8	30	8	30	58.6	26.35	101.25	10	5.6
2008	8	31	8	31	12.2	26.27	101.75	10	5.6
2008	9	3	6	27	25.47	24.87	97.78	10	5
2008	9	10	1	14	31.88	30.78	83.59	10	5.3
2008	9	10	1	28	6.09	30.80	83.40	7.3	5.4
2008	9	22	13	30	38.18	15.58	96.08	35	5.2
2008	9	25	1	47	11.19	30.84	83.49	4	6
2008	10	5	15	52	46.2	39.80	73.64	33	6.4
2008	10	5	22	56	28.3	33.89	69.34	10	5.7
2008	10	6	8	30	45	29.84	90.36	10	6.1
2008	10	6	12	46	45.7	30.40	90.97	10	5
2008	10	8	14	7	16.29	29.76	90.33	9	5.5
2008	10	13	17	16	18.7	38.20	70.53	25.2	5.3
2008	10	28	22	33	8.5	30.58	67.42	10	5.5
2008	10	28	23	9	57.2	30.49	67.43	10	6.2
2008	10	29	11	32	31.9	31.08	66.65	15	6.2
2008	10	30	7	16	21	30.18	67.55	10	5
2008	10	31	23	59	52.92	30.54	67.44	10	5.1
2008	11	11	21	56	3.9	37.31	95.37	10	5.4
2008	11	16	12	20	36.88	10.83	91.71	26.7	5.5
2008	12	8	8	59	11.32	29.95	82.05	35.6	5.3
2008	12	9	2	46	32.72	30.34	67.56	10	5.2
2008	12	9	12	57	18.01	30.31	67.64	10	5.2
2008	12	9	18	53	14.4	32.49	104.93	20	5.6
2008	12	9	22	52	37.62	30.44	67.40	10	5.7
2008	12	11	12	31	5.42	35.31	81.41	10	5
2008	12	20	23	22	48.38	22.75	95.90	10	5.3
2009	1	21	1	42	24.65	15.65	96.04	35	5
2009	1	28	0	1	16.5	0.15	98.50	20	5.8
2009	2	2	8	36	48	27.12	66.18	33	5.1
2009	2	18	10	11	43.65	30.67	83.86	35	5.1
2009	2	23	5	56	30.9	0.46	98.66	33	5.7
2009	3	14	13	26	23.04	30.15	68.47	35.5	5
2009	3	17	23	14	46.9	25.79	67.44	13.6	5
2009	4	1	2	34	31.8	34.02	82.67	10	5.2

2009	4	30	10	4	24.5	27.65	61.72	10	5.7
2009	5	10	17	34	7.8	38.16	67.97	10	5.4
2009	6	4	2	54	44.1	33.31	82.08	10	5.1
2009	6	17	4	12	51.79	21.72	62.04	10	5
2009	6	29	18	3	51.1	31.60	103.92	10	5.2
2009	7	9	11	19	11.6	25.46	101.60	15	5.5
2009	7	10	9	2	3.7	25.67	101.03	10	5
2009	7	24	3	11	55.7	31.16	86.04	10	5.7
2009	7	27	6	23	36.8	35.56	72.54	10	5.1
2009	8	9	4	2	7.3	35.58	81.65	10	5.1
2009	8	10	19	55	37.5	14.10	92.83	10	6.9
2009	8	13	9	21	34.8	14.12	92.65	13.3	5.7
2009	8	28	1	52	0.6	37.99	96.20	10	6.2
2009	8	31	10	15	32.8	37.50	95.59	10	5.8
2009	8	31	21	51	42	37.36	95.56	10	5.2
2009	10	16	19	29	14.1	35.04	92.11	10	5
2009	10	25	11	40	49.1	34.84	80.60	10	5
2009	10	30	6	43	3.83	34.18	70.02	30.4	5.1
2009	11	7	20	8	45.9	29.66	85.90	10	5.6
2009	11	14	22	2	45.51	5.90	61.22	10	5.3
2009	11	27	16	4	4.5	31.29	103.68	10	5.1
2009	12	21	5	15	12.3	37.31	96.36	10	5.3
2010	2	25	4	56	51.9	25.35	102.03	10	5.1
2010	3	14	19	9	5.6	35.30	74.50	43.6	5.2
2010	3	24	2	6	9.4	32.58	92.64	10	5.5
2010	3	24	2	44	47.4	32.68	92.95	10	5.6
2010	3	30	16	54	46.73	13.67	92.83	34	6.6
2010	4	1	14	7	30.89	30.09	69.54	35	5
2010	4	6	22	15	2.7	2.44	97.01	33	7
2010	4	13	21	39	56.1	33.26	96.87	10	5.2
2010	4	14	1	25	14.9	33.23	96.45	10	5.8
2010	4	17	0	58	58.6	32.51	92.83	35	5.3
2010	4	18	20	28	43.2	36.03	67.00	10	5.6
2010	4	28	18	1	21.25	19.39	93.16	35.9	5.2
2010	5	9	5	59	39.8	3.66	96.19	33	6.5
2010	5	11	12	17	45.8	3.65	96.19	33	5.6
2010	5	14	14	46	29.8	29.58	90.16	10	5
2010	5	25	6	11	56.3	30.97	103.01	10	5.3
2010	5	29	2	29	46.4	33.25	96.32	10	5.5
2010	6	3	5	35	44.1	33.28	96.07	10	5.2
2010	6	5	16	59	15.93	28.17	65.97	10	5
2010	6	12	19	26	50.46	7.88	91.94	35	7.5
2010	6	18	23	9	31.02	13.20	93.09	20	5.9
2010	6	22	23	14	10.84	29.87	80.43	16.3	5.2
2010	6	24	4	8	35.06	7.70	91.96	20.5	5.5
2010	7	6	19	8	25.87	29.84	80.40	32.8	5
2010	8	14	20	18	2.28	28.33	66.32	35	5.2
2010	8	21	5	42	55.5	2.39	96.82	34.4	5.5
2010	9	7	15	41	36.9	39.62	73.73	10	5.5
2010	9	7	20	50	56.6	33.30	96.33	10	5

2010	9	10	17	24	16.61	23.41	90.65	10	5.1
2010	9	11	11	43	8.6	7.79	94.06	10	5.8
2010	9	30	9	3	4.3	4.76	95.05	33	5.5
2010	10	6	17	49	42.5	29.67	69.47	10	5.1
2010	11	15	0	51	47.3	35.02	69.85	33	5.2
2010	11	30	8	39	54.1	30.14	90.53	10	5.4
2010	12	9	23	17	32.8	31.54	70.03	10	5.1
2010	12	11	15	34	27.7	30.27	69.34	10	5.1
2010	12	21	14	7	48.2	2.79	96.14	27.1	5.6
2010	12	29	18	30	56.8	30.97	86.82	10	5.2
2011	1	1	1	56	3.5	39.70	75.05	10	5
2011	1	1	23	33	39.49	24.65	97.92	21.4	5
2011	1	18	20	23	19.9	28.70	63.83	27	6.8
2011	1	19	3	47	4.5	39.80	72.93	33	5
2011	1	24	2	45	26	38.51	73.13	33	6
2011	2	1	13	39	43.4	10.54	94.32	10	5.5
2011	2	4	13	53	41.2	24.93	94.80	33	6.4
2011	3	10	4	58	13.75	24.73	97.96	10	5.5
2011	3	24	13	55	12.01	20.69	99.82	8	6.9
2011	3	25	0	22	39.2	20.81	99.93	10	5
2011	4	4	11	31	43.05	29.70	80.75	26.1	5.3
2011	4	6	14	1	44.5	1.77	97.06	20.3	5.9
2011	4	10	9	2	48.5	31.30	100.46	43	5.1
2011	4	19	16	27	26.81	34.29	89.58	15.1	5
2011	6	3	0	53	27.28	27.53	88.02	45.7	5
2011	6	14	3	1	27.6	1.89	99.36	15.8	5.5
2011	6	20	10	16	53.6	25.19	98.56	12.3	5.4
2011	6	26	7	48	11.3	32.73	96.27	29	5.2
2011	7	24	10	38	54	28.27	66.37	10	5
2011	8	1	19	40	53.48	33.74	87.57	13.6	5.1
2011	8	10	0	53	21.6	27.67	65.11	10	5.7
2011	9	8	19	46	44.3	39.32	70.58	12.9	5.1
2011	9	15	15	27	13.7	35.56	82.61	39.7	5.2
2011	9	18	12	40	46.9	27.85	88.06	45.9	6.7
2011	11	30	19	42	34.43	7.80	93.86	17	5.6
2011	12	23	12	2	1.9	28.84	68.20	14.4	5.1
2012	1	10	18	36	59.1	2.43	93.14	11.2	6.7
2012	2	9	19	17	30.55	30.99	78.28	6.2	5.1
2012	2	17	15	44	23.23	32.39	82.79	21.9	5.2
2012	2	20	13	59	23.79	35.72	79.72	10	5
2012	3	5	7	41	4.53	28.81	76.65	10	5.1
2012	3	6	2	52	40.2	8.34	93.79	17	5.5
2012	3	12	6	6	40	36.83	72.75	13.6	5.7
2012	3	27	23	40	12.6	26.09	87.78	28.8	5
2012	4	15	5	57	38.6	2.53	90.30	15	6.2
2012	4	24	9	50	58.39	5.65	61.51	10	5.6
2012	4	24	14	57	8.6	8.73	94.08	14	5.5
2012	4	30	8	0	9.4	1.61	89.51	14	5.5
2012	5	11	12	41	35.3	26.18	92.89	43.3	5.4
2012	5	12	23	28	42.3	38.66	70.14	15	6

2012	6	11	5	2	16	35.84	69.29	29	5.3
2012	6	19	20	14	2.3	23.62	70.23	17.5	5.4
2012	7	22	2	11	12.21	25.00	96.43	22.6	5.1
2012	7	25	0	27	43.7	2.71	96.12	11.6	6
2012	8	13	20	32	55.6	35.18	73.57	20	5.4
2012	8	23	16	30	21.79	28.47	82.69	28.4	5
2012	9	7	3	19	42.2	27.56	103.96	10.6	5.6
2012	9	7	4	16	33	27.57	103.69	10	5.6
2012	9	13	8	17	54.3	30.01	70.09	10	5.1
2012	10	2	18	37	38.7	26.88	92.82	36.8	5.2
2012	10	18	2	33	27.97	23.77	81.31	10	5
2012	11	11	1	12	38.87	23.01	95.89	13.7	6.8
2012	11	11	10	54	41.35	22.72	95.83	6	5.8
2012	11	11	18	19	45.08	23.13	95.87	28.4	5.5
2012	11	19	17	54	7.46	30.54	67.58	10	5.3
2012	12	25	17	36	32.8	28.46	66.47	35	5
2013	1	30	9	27	3.6	32.93	94.67	20.1	5.2
2013	2	25	5	11	8	34.28	85.65	12.6	5.4
2013	3	2	1	30	39.3	24.67	92.23	45.8	5.2
2013	3	3	5	41	16.9	25.97	99.80	8	5.2
2013	4	3	16	35	45.1	19.22	95.65	6	5.4
2013	4	4	15	16	28.4	19.25	95.74	22.4	5.1
2013	4	16	8	34	12.9	28.87	95.12	31.7	5.3
2013	5	1	6	57	12.7	33.10	75.84	9.8	5.7
2013	6	28	11	40	47.4	28.74	82.30	10	5
2013	8	2	21	37	46.6	33.37	75.88	47.52	5.2
2013	8	6	15	31	22.55	31.45	86.43	11.92	5.2
2013	8	11	21	23	43.81	30.08	97.93	19.66	5.7
2013	8	12	8	9	38.3	30.13	97.94	9.57	5
2013	8	31	0	4	18.01	28.23	99.37	9.75	5.8
2013	9	24	11	29	47.97	26.95	65.50	15	7.7
2013	9	24	17	20	13.52	27.13	65.47	10.52	5.5
2013	9	28	7	34	6.45		65.51	12	6.8
2013	10	18	13	18	22.34	28.26	66.49	10	5.3

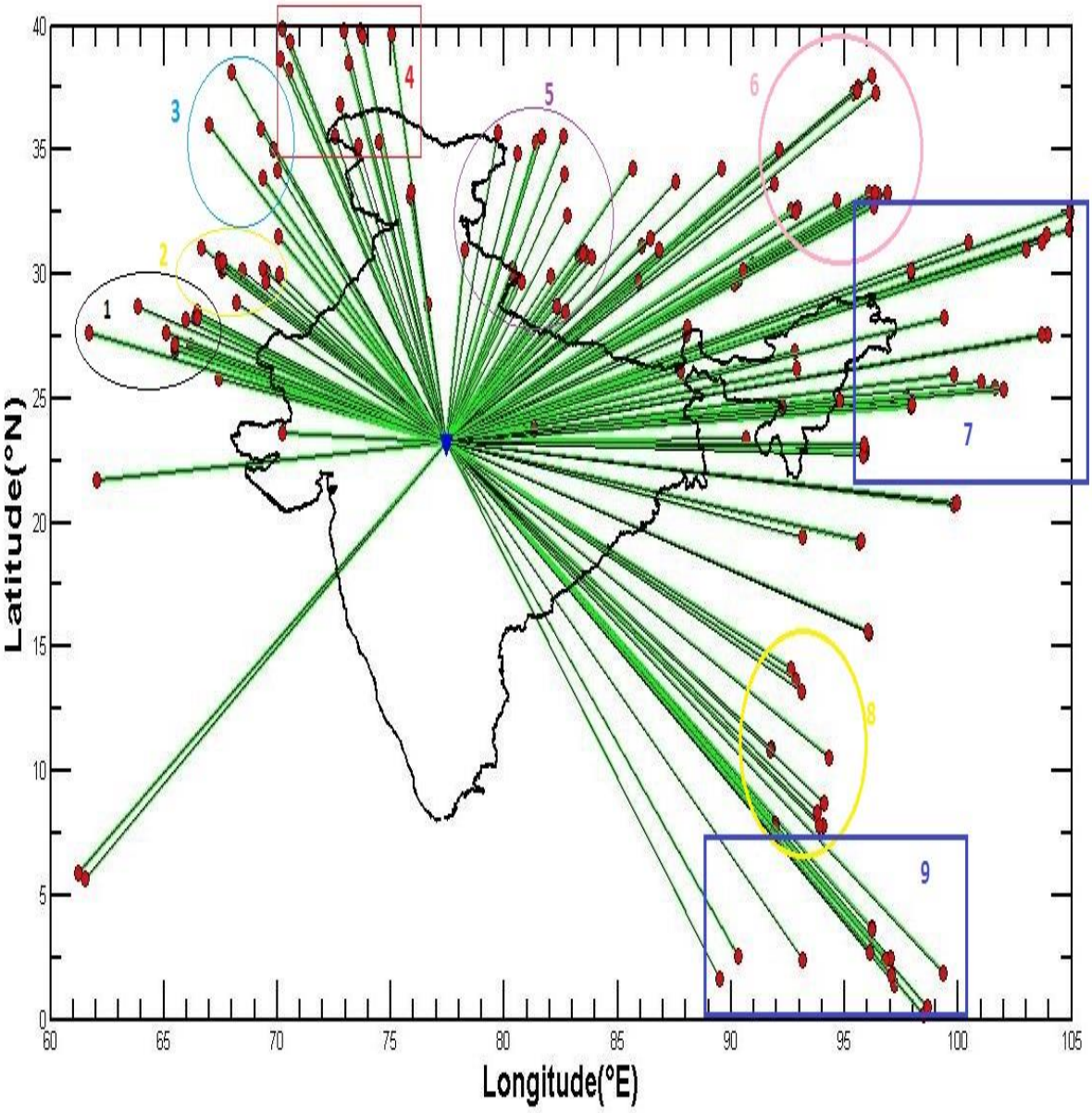

Figure 6.1. The coverage map of the events with respect to India

CHAPTER #7 METHOD FOR DISPERSION CURVE

7.1. Data pre-processing

The data for the station was extracted from the Indian Metrological Department database for BBS network of India. These were cross referenced with the event catalog to obtain the required data and those signals for which event was cataloged was separated out. Data with poor signal to noise ratio were removed by visual inspection as well as application of several filters vis Seisan software (Havskov and Ottemoeller, 2005) using mulplt command. Those events for which appreciable signal can be observed were cut with 2 minutes before the event and 30 minutes post event so as to get complete surface wave information.

These extracted events were examined for any header discrepancies and if so these were fixed through wavfix tool of Seisan. As for the analysis for the surface wave I used GSAC software developed by Herrmann (2002). The data files were in Seisan format. They were converted into SAC format using sacsei command of Seisan. Once the file was converted to SAC file format, all the operations after that were done using GSAC. The latitude and longitudes of the stations, coordinates of the events and origin times of events were modified in the header of file using ch command of GSAC. The origin time gives the o- marker in the signal and thus calculates the distance between the event location and station location. These steps prepare the raw data for further processing to obtain dispersion curves using Multiple Filter Techniques (Hermann, 2002). After correcting the header information for the seismographs, mean, and trend were removed using predefined function available in GSAC. Further a symmetric taper is applied to each end of data to avoid spectral leakage in frequency domain. Then instrument correction is applied for using transfer function using the pole-zero file prepared. Table 7.1. Show the pole zero file used in my operation. After correcting for instrument response, the signal is rotated through great circle path to get vertical, radial, and transverse components.

Table 7.1. SAC Poles and zeros file used for BBS network

ZEROS 5
0.0 0.0
0.0 0.0
-91.66 0.0
-160.10 0.0
-3207.0 0.0
POLES 7
-0.01770 0.01760
-0.01770 -0.01760
-126.70 0.0
-192.0 259.10
-192.0 -259.10
-557.70 1143.0
-557.70 -1143.0
CONSTANT 2.7102E+12

7.2. Processing and Dispersion curves extraction

do_mft

The major time consuming part of multiple filter analsysis is to manualy select the correct dispersion from the program output. This was made easier by the application of do_mft module which permits the selection of SAC files to process, defining the trace units and filter parameters, interactive identification of modes, choice of match filtering and saving of processing results. One start the program with the simple command.

do_mft *

Where by the program looks at all files in the current directory to determine whether they are SAC files. The result is the initial screen

Do MFT Steps

The following process is done for event occurred on 2005-02-18-1932, the subsequent seismogram fro this is as follows

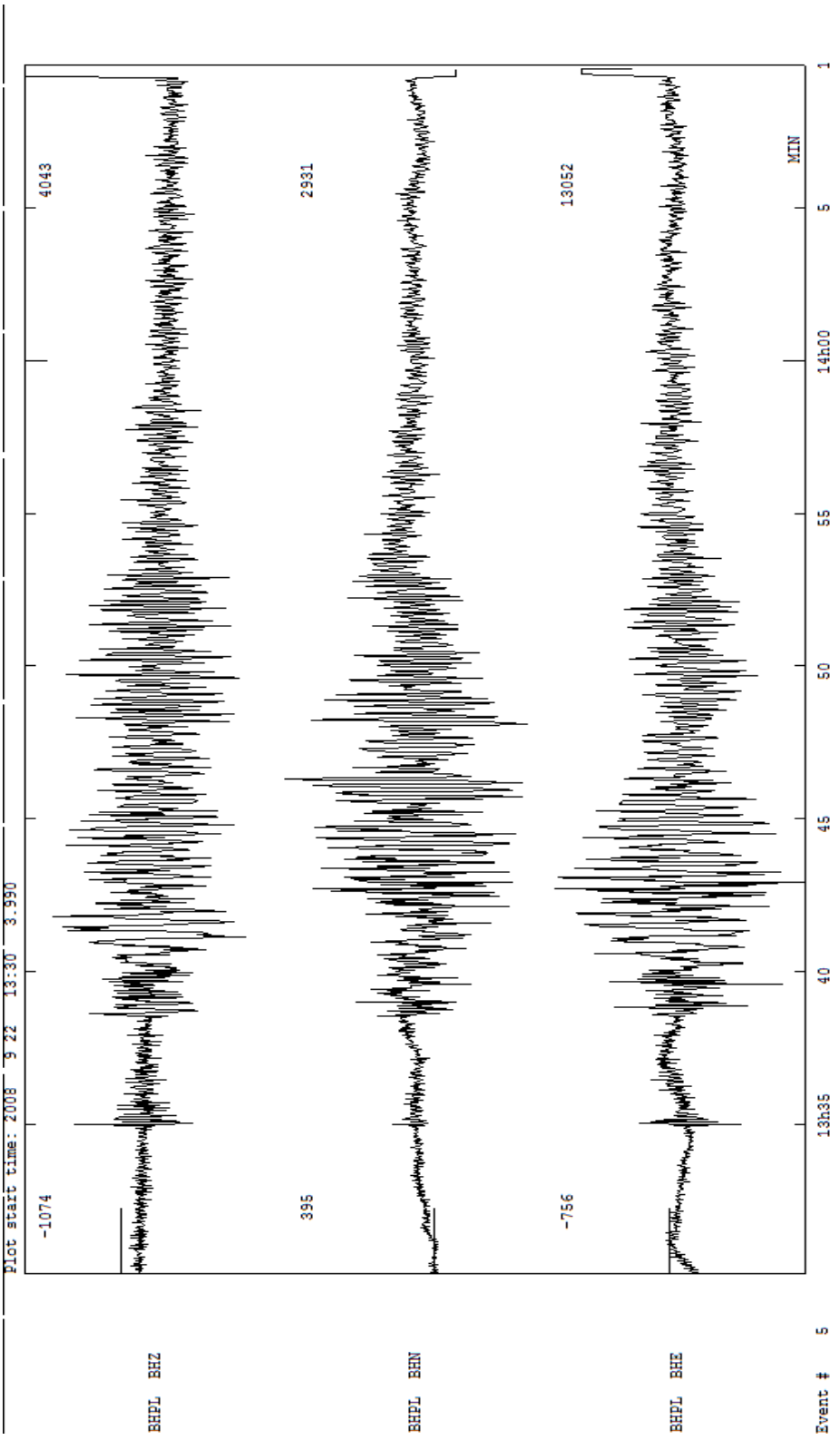

Figure 7.1. Signal recorded at Bhopal station 2008-09-22 13:30 3399

The steps followed to obtain the dispersion curves for Rayleigh waves using do_mft(Herrmann,2002) has been illustrated in Figure 7.1.

(a)

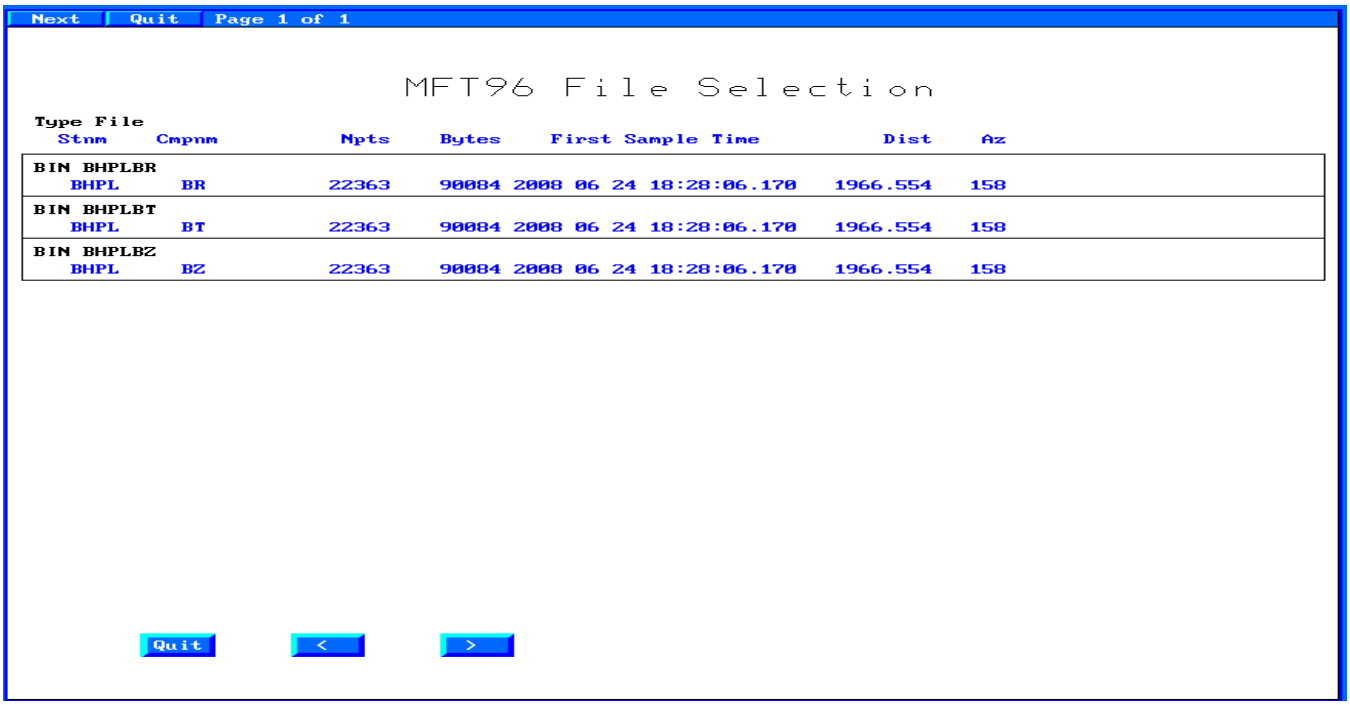

(b)

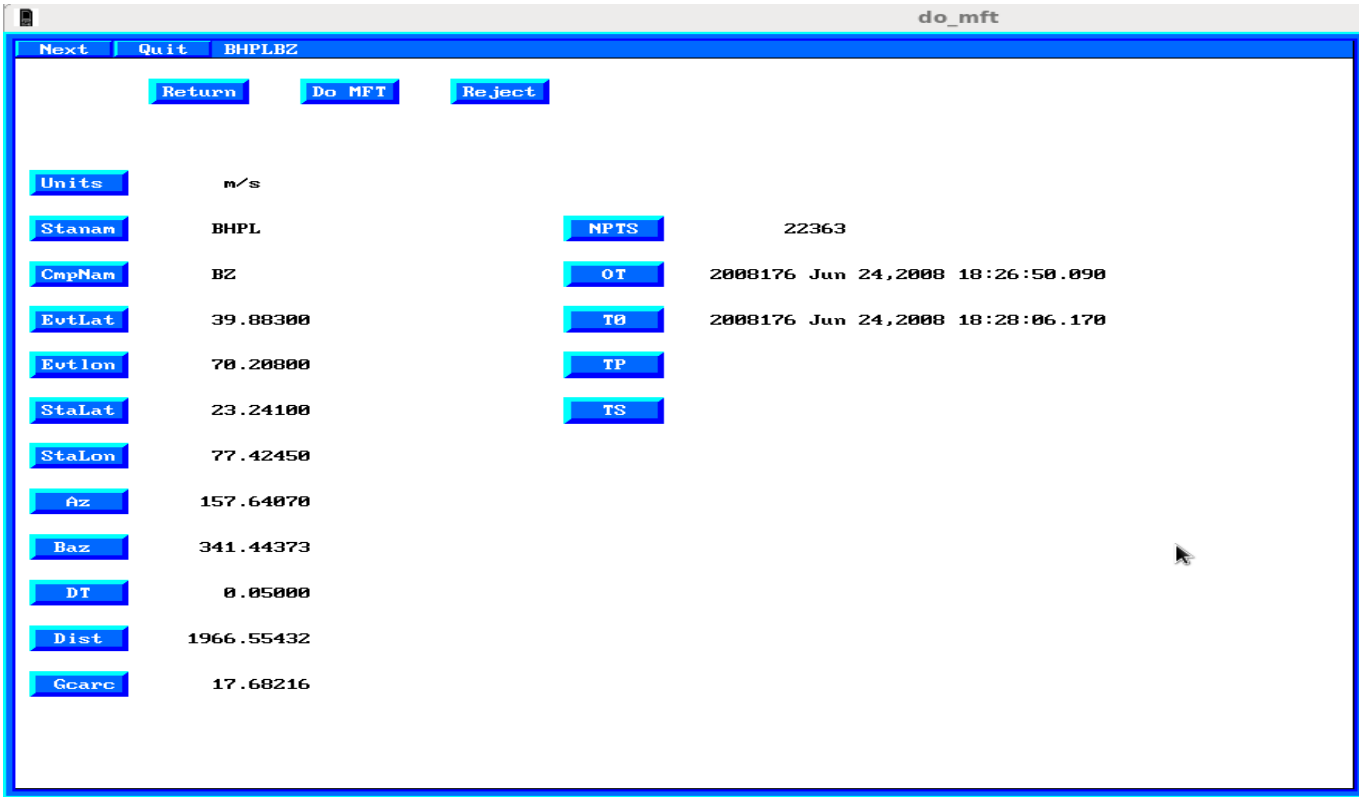

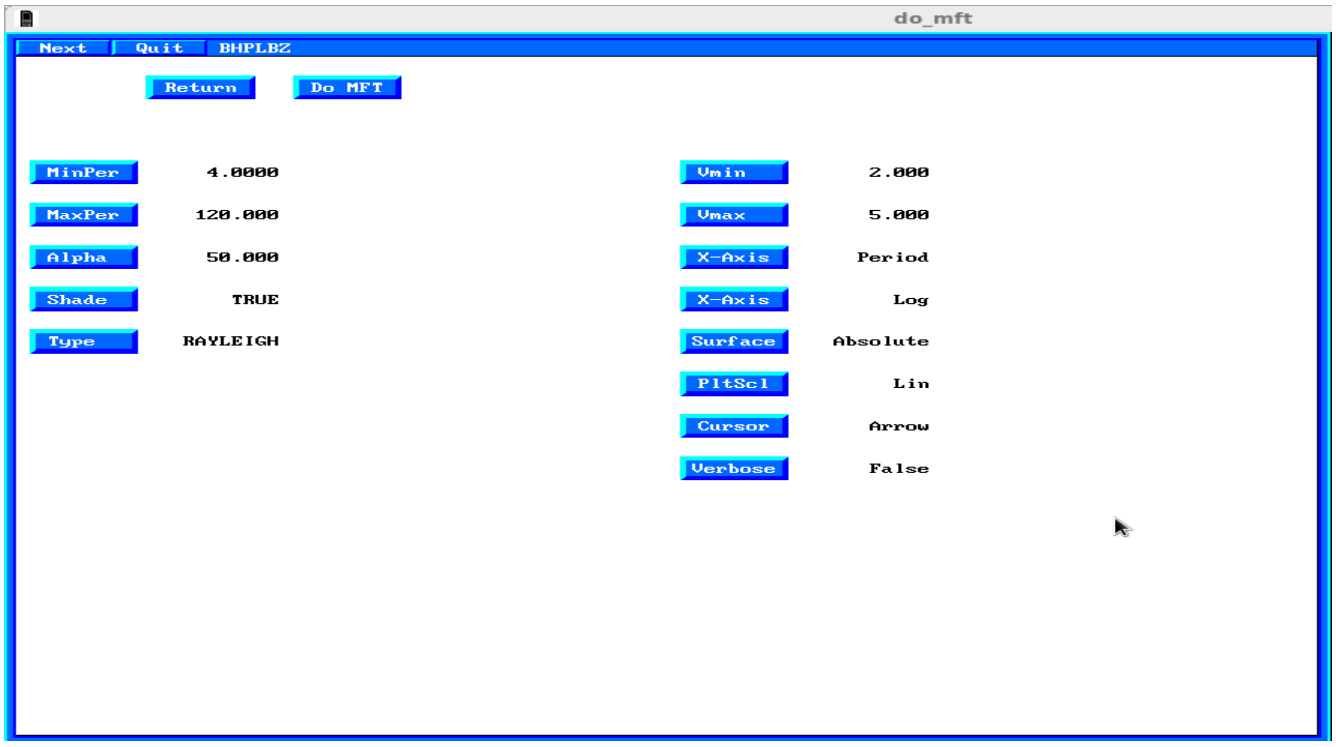
do_mft
Next
Quit
BHPLBZ
Return
Do MFT
MinPer
4.0000
MaxPer
120.000
Alpha
50.000
Shade
TRUE
Type
RAYLEIGH
Vmin
2.000
Vmax
5.000
X-Axis
Period
X-Axis
Log
Surface
Absolute
PltScl
Lin
Cursor
Arrow
Verbose
False

(d)

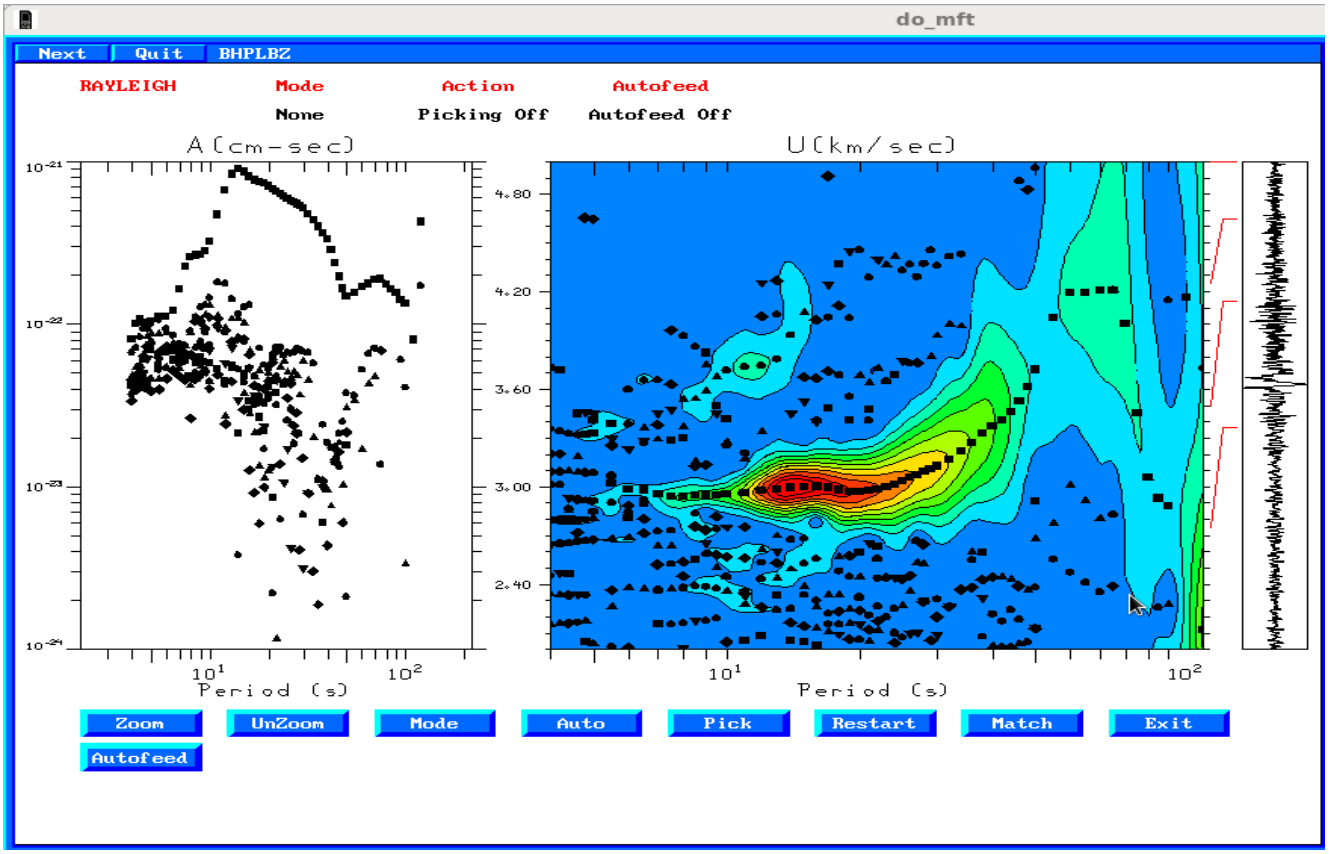
do_mft
Next
Quit
BHPLBZ
RAYLEIGH
Mode
None
Action
Picking Off
Autofeed
Autofeed Off
A (cm-sec)
U (km/sec)
Period (s)
Period (s)
Zoom
UnZoom
Mode
Auto
Pick
Restart
Match
Exit
Autofeed

(e)

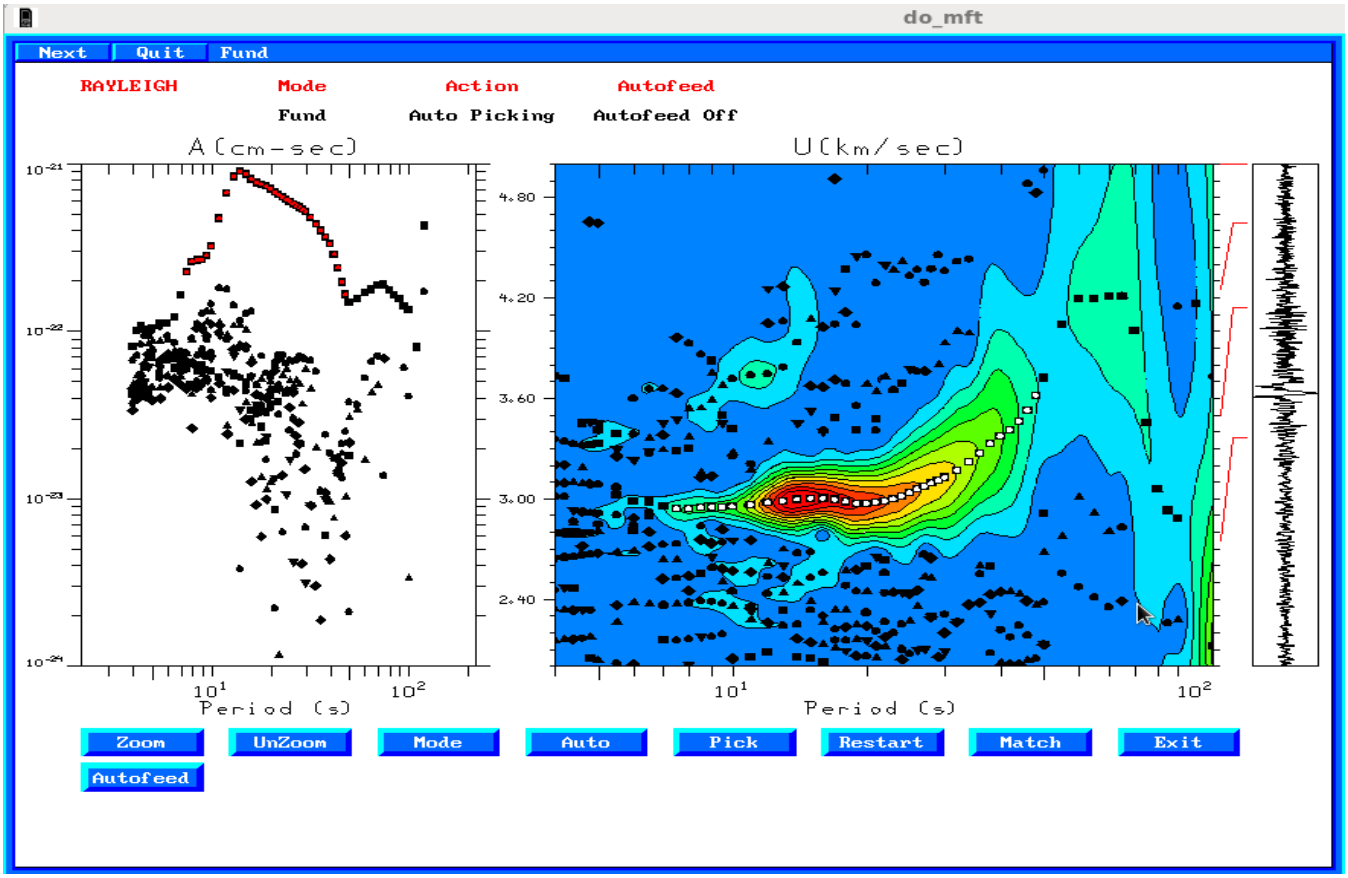
do_mft
Next
Quit
Fund
RAYLEIGH
Mode
Fund
Action
Auto Picking
Autofeed
Autofeed Off
A (cm-sec)
U (km/sec)
Period (s)
Period (s)
Zoom
UnZoom
Mode
Auto
Pick
Restart
Match
Exit
Autofeed

(f)

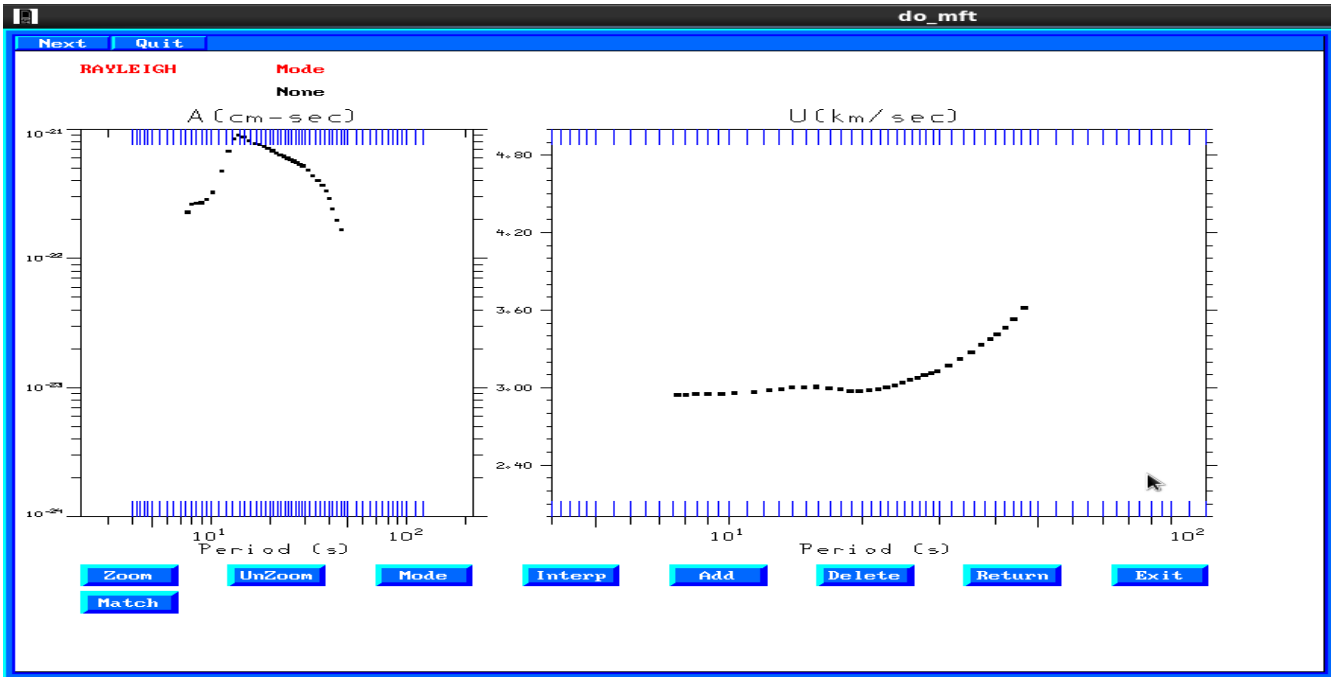
do_mft
Next
Quit
RAYLEIGH
Mode
None
A (cm-sec)
U (km/sec)
Period (s)
Period (s)
Zoom
UnZoom
Mode
Interp
Add
Delete
Return
Exit
Match

(g)

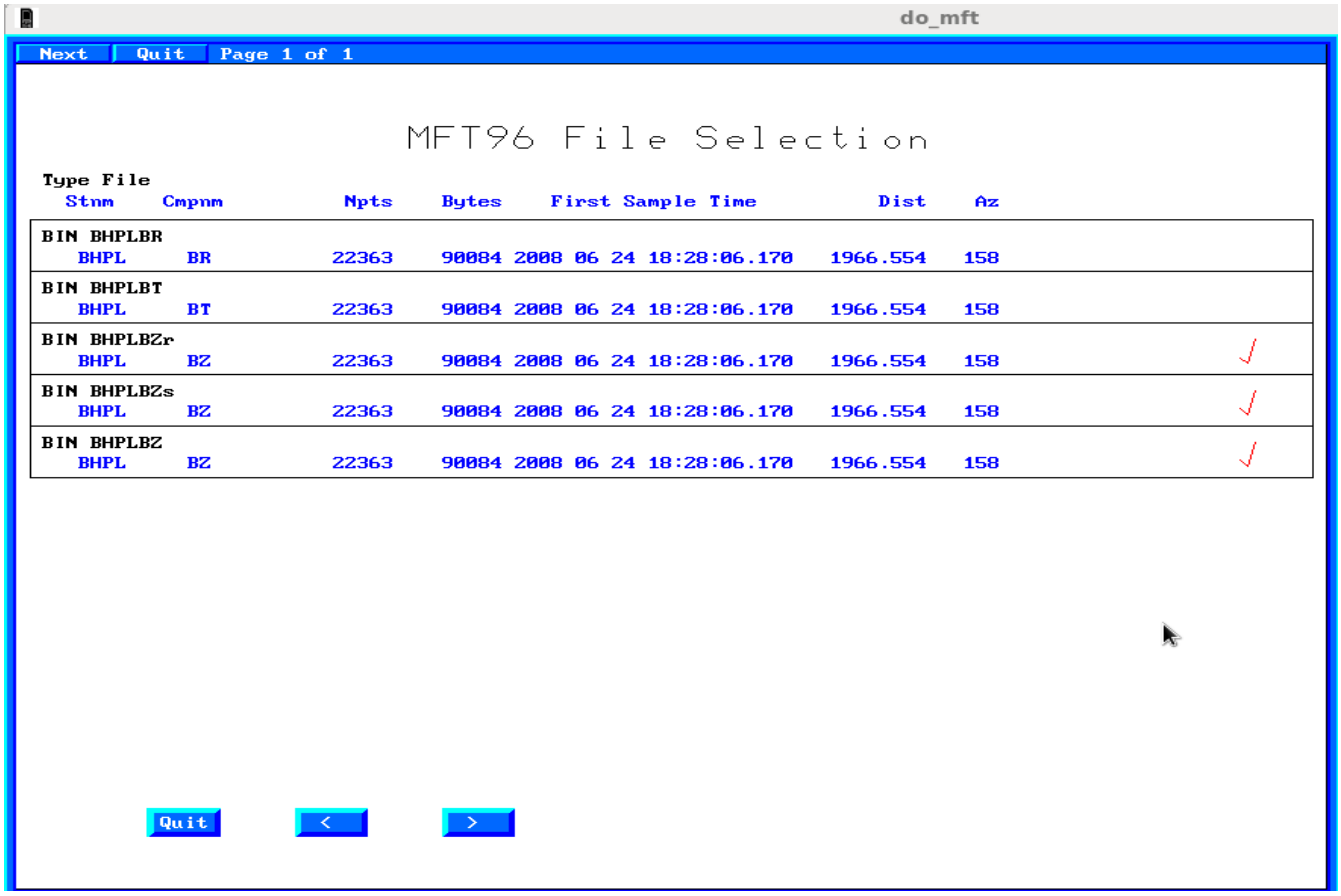

Figure 7.2. (a) The initial screen that is visible when the program starts. (b) The second screen permits one to define the units and to review, but not change, the contents of the SAC header. The DIST is required. (c) Selecting the Do MFT button, leads to the next stage, whereby one can change the periods for processing, the filter parameter and, the shading, and the wave type (UNKNOWN, LOVE or RAYLEIGH), and the plotting parameters. If the do mft is again pressed, the program sacmft96 is run in the background to create three files: the dispersion file, the graphic plot, and an index file to the graphic. do_mft displays this together with processing buttons . (d) The next screen execute the MFT program and we can see a dispersion contours. Since we have taken the Rayleigh wave mode initially the subsequent plot for Rayleigh waves. (e) Next step is to pick the fundamental mode values from the dispersion curves as follows so to define the mode and then select the dispersion values a single point at a time, Pick or by finding values near a connected line, Auto. If desired one move to the phase match filter stage, Match . (f) After which requires the specification of a single mode. After phase match filtering the initial file menu is updated so that one could perform the multiple filter analysis on the presumably single mode trace.

The same steps are repeated for Love wave as well.

Love wave

For Love waves steps 1 and 2 remains same as Rayleigh wave, In step 3 we need to select type as Love as shown in Figure 7.3.

(a)

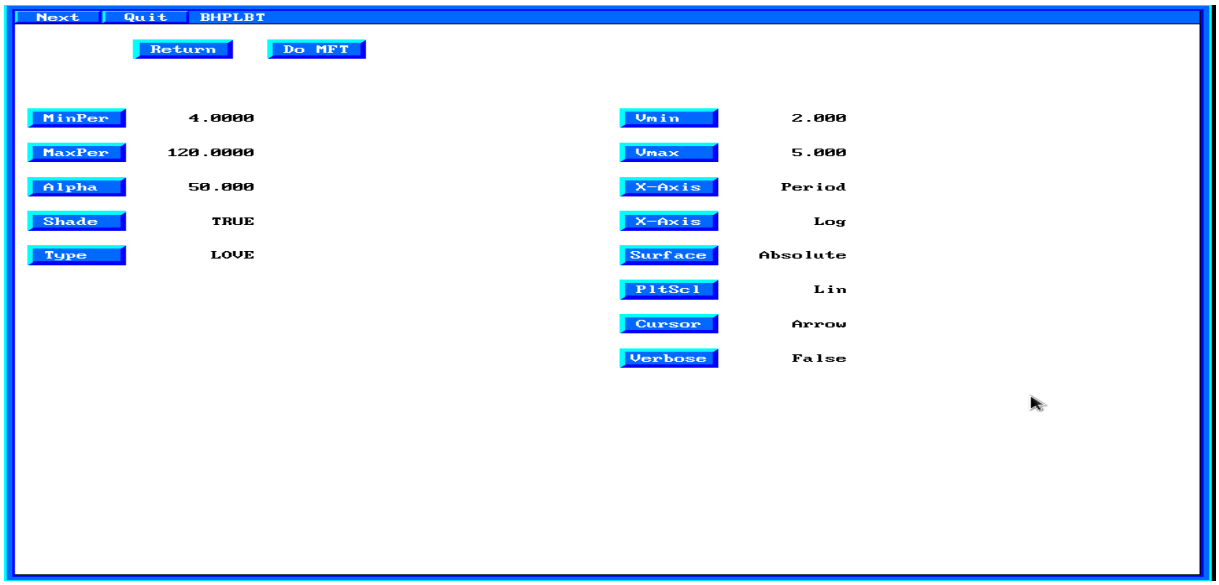

(b)

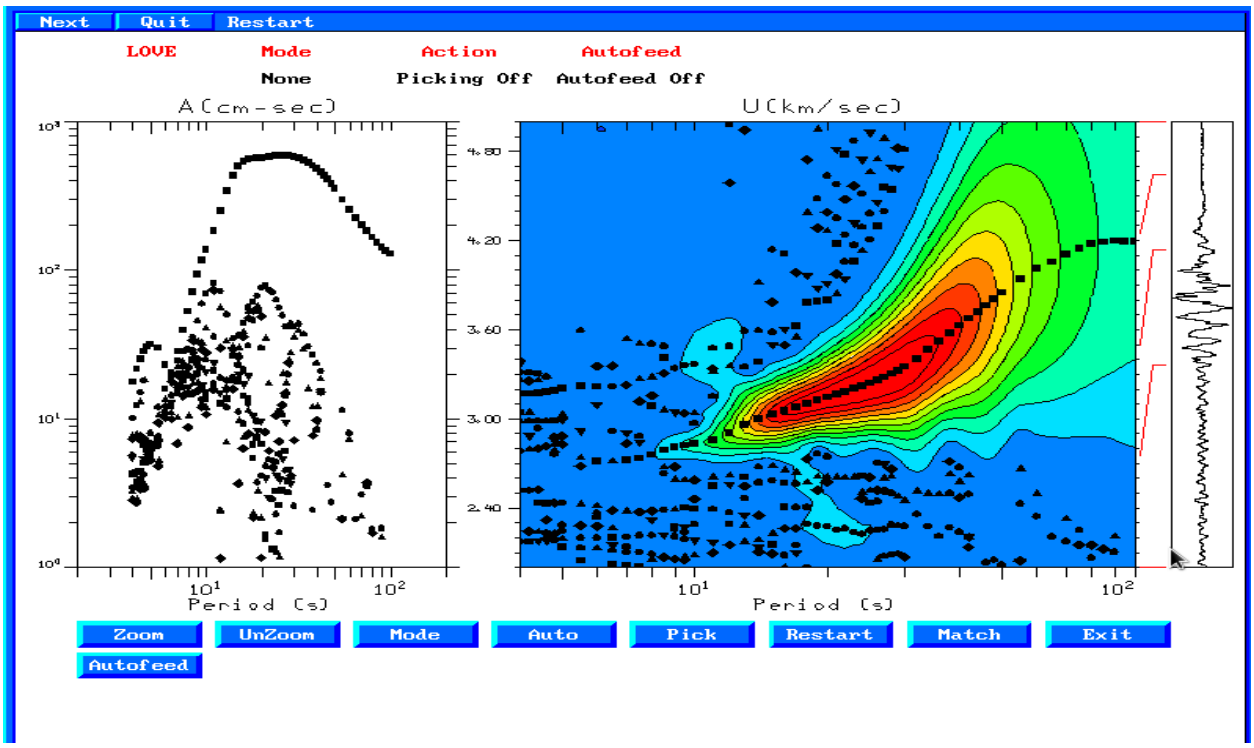

(c)

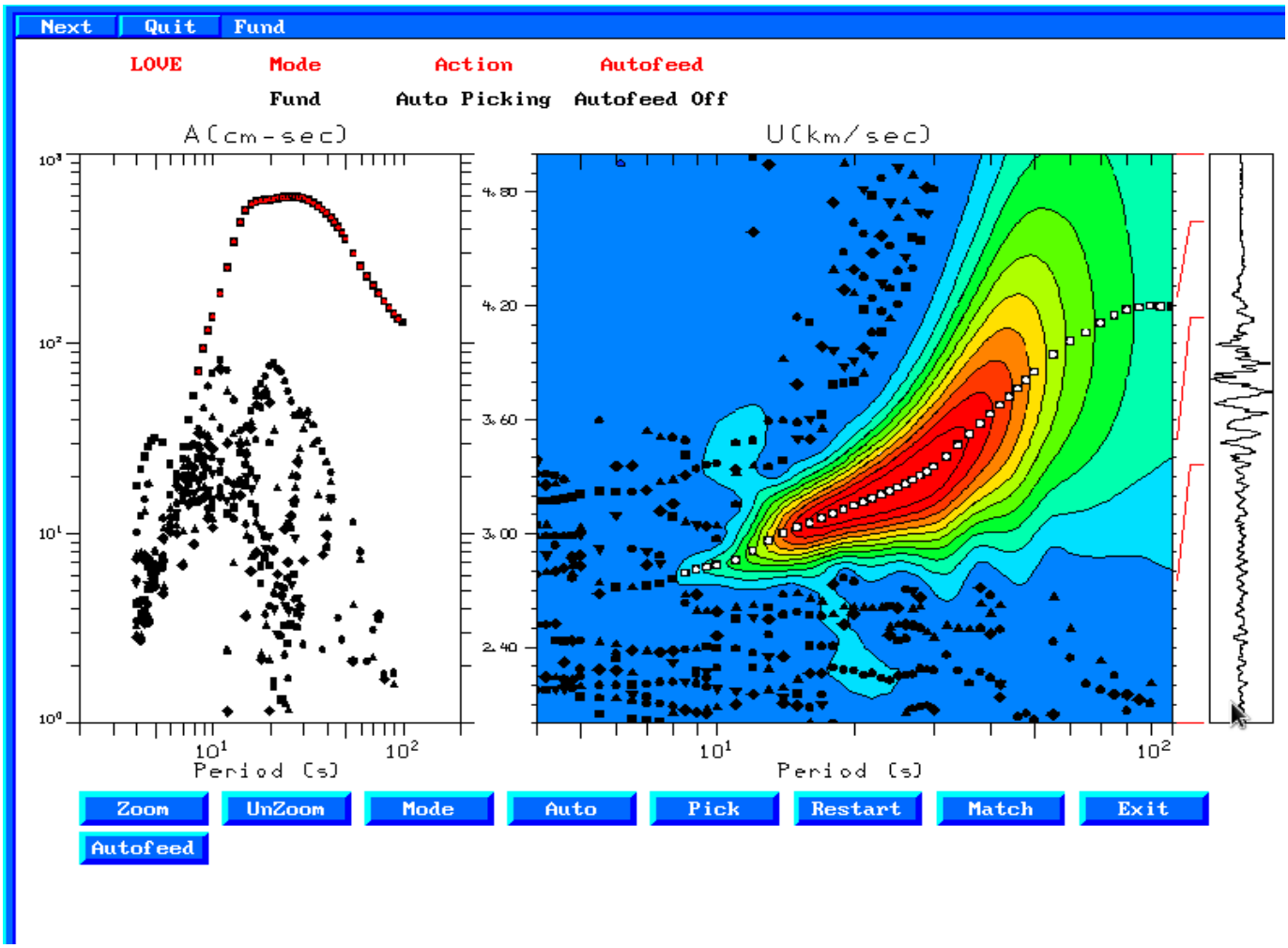
Next
Quit
Fund
LOVE
Mode
Action
Autofeed
Fund
Auto Picking
Autofeed Off
A(cm-sec)
U(km/sec)
Period (s)
Period (s)
Zoom
UnZoom
Mode
Auto
Pick
Restart
Match
Exit
Autofeed

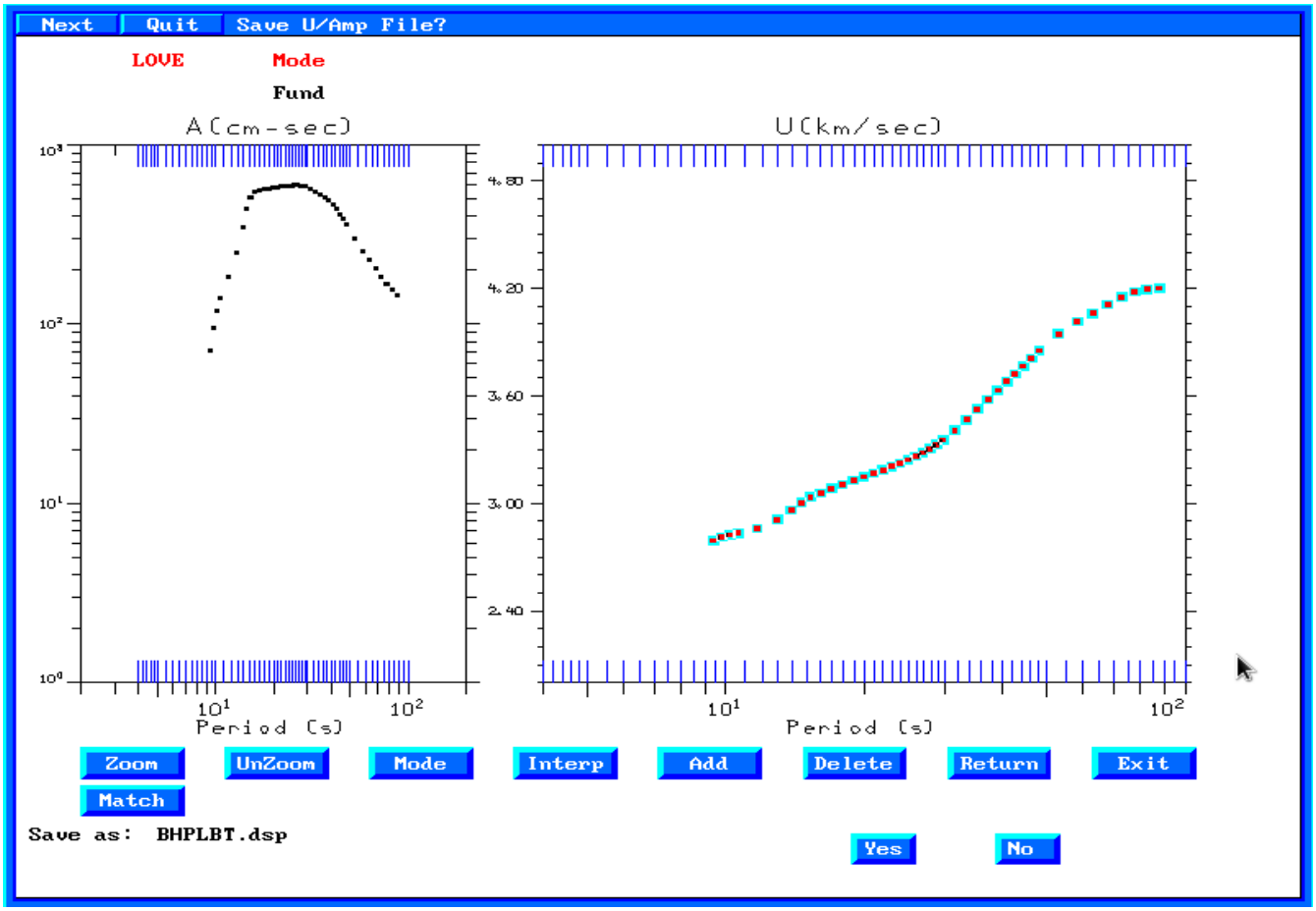

Figure 7.3. (a) Selection of Love wave in type of wave to obtain dispersion. (b) The dispersion plot is shown. (c) Interactively I have chosen the fundamental mode dispersion values.

Thus after completing the do_mft operation we obtain dispersion values.

7.3. Averaging of the dispersion curves

The curves for group velocity versus period obtained for each events from dispersion curves using MFT is stored. These values appears to be scattered so to fit a polynomial we need to average out the group velocities at a specific time in period. Thus we use weighted average method of averaging out before fitting a fifth order polynomial to it. The subsequent plots resulted from polynomial fit with the original curves are shown later.

CHAPTER#8 METHOD FOR INVERSION

To do the procedure of inversion we have used the surf96 module by R.Herrmann. Before proceeding further to the application of the codes we will be requiring an initial model. Souriau, 1981 proposed that the region should be modeled through three different initial models. These models will partly cancel the bias crept in due to epicenter mislocations, poor model information due to path corrections and error in origin time.

8.1. Bay of Bengal Model

INDSD-model proposed by Gabriel and Kuo(1966) has been used for continental path. A mean sediment thickness of 8km has been assumed (Heezen et al., 1976). It has been supposed that the Moho depth remains unchanged by this sediment cover. The water depth is at 3.3km according to bathymetric map. Hamilton and Bachman (1977) gave the sediment thickness and P-velocities derived from the analogy of Arabian Fan (Bachman and Hamilton, 1980) at a depth more than 1km. Rao and Rao (1974) proposed the existence of a thin crust with possibility of higher Pn and Sn velocities. Further if we take into the presence of Ninety-east ridge into consideration the upper mantle structure represent a closer association with old ocean model from regionalization of great circle Rayleigh wave given by L*éve*que(1980).

Table 8.1. The initial model of Bay of Bengal

Layer N	h(km)	P-velocity(km/s)	S-velocity(km/s)	Density(g/cm^3)	Q_P	Q_S
1	0.5	1.7	0.9	1.8	43	30.351
2	0.5	2.2	1.15	2	43	29.97
3	4.5	3	1.7	2.3	43	32.483
4	3	6.8	3.9	2.85	43	32.893
5	5	8.2	4.75	3.2	43	33.217
6	6.5	8.2	4.75	3.2	43	33.217
7	10	7.9	4.73	3.3	43	34.331
8	10	7.9	4.73	3.3	43	34.331
9	10	7.8	4.51	3.4	43	33.159
10	10	7.8	4.51	3.4	43	33.159
11	10	7.8	4.42	3.4	43	32.483
12	10	7.8	4.42	3.4	43	32.483
13	10	7.8	4.42	3.4	43	32.483
14	10	7.8	4.42	3.4	43	32.483
15	Half space	7.8	4.33	3.4	60	44.42

8.2 NORTH-EAST INDIA MODEL

This model is given by Supriyo Mitra et al. (2003). This study is based on the receiver function. This study shows that beneath Shillong Plateau crust is thinnest (~35– 38 km). Moho under the northernmost Bengal Basin is at a depth of~44 km indicated by receiver function from southern backazimuth events. But northern backazimuth events indicate Moho under southernmost Shillong Plateau is at a depth of ~38 km. On the BrahmaputraValley Receiver functions demonstrate that Moho is deeper by~5–7km than below the Shillong Plateau.

Table 1. Station name, location, backazimuth and delta bins and number of receiver functions stacked, average crustal V_s and crustal thickness obtained from the inversion of receiver functions for the stations used in this study. CHP is given twice for the events from the northeast (CHP-N) and southeast (CHP-S).

Station	Lat. (°N)	Long. (°E)	BAZ (°)	Δ(°)	No. of RFs	V_s (km s^{-1})	Moho depth (km)
KMG	24.8466	92.3435	38–42	60–68	2	3.53	39
CHP-S	25.2806	91.7235	106–125	45–66	9	3.63	44
CHP-N	25.2806	91.7235	52–86	36–48	6	3.76	38
SHL	25.5663	91.8558	86–109	51–65	3	3.77	35
BPN	25.6698	91.9088	52–72	44–48	3	3.76	35
GAU	26.1500	91.6500	302	21	2	3.63	40
BAI	26.3183	91.7399	107–117	67–76	10	3.86	42
TEZ	26.6333	92.8333	89–130	37–57	7	3.83	42
BMD	27.2713	92.4181	90–119	51–61	10	3.58	48
SP27	27.6712	89.0762	50–55	48–54	12	3.62	62
SP25	28.1778	89.3029	50–55	47–53	15	3.72	68
BB23	28.4856	89.6585	44–55	47–54	6	3.63	62
BB20	28.7273	89.6643	145–146	39–45	5	3.65	76
BB18	28.9301	89.7440	145–146	39–45	4	3.61	76
BB14	29.3682	90.1845	44–57	46–54	12	3.65	80
LSA	29.7000	91.1499	42–129	40–55	30	3.74	88

8.3 Velocity structure of North western Indian Peninsular Shield

This model is given by Gaddale Suresh et al. (2015) on the basis of inter-station phase velocities of Rayleigh and Love waves. The phase velocities of Rayleigh waves are in the period range of 10 to 275 s and for Love waves it is 10 to 120 s . Through inversion of the phase velocities the isotropic model obtained indicates 199.1 km thick lithosphere with 3 layered crust of thickness 36.3 km. The top two layers have almost same velocities and both constitute the upper crust with thickness of 12.6 km. The upper crust is mafic, whereas the lower crust is felsic. In the mantle lid, velocities increase with depth.

Layer no.	Search range			Accepted structure			
	Thickness (km)	V_S (km/s)	V_P/V_S	Thickness (km)	V_S (km/s)	V_P (km/s)	Depth of top layer (km)
1	04 - 08	3.0 - 3.4	1.7 - 1.85	05.9±0.6	3.335±0.031	6.155±0.058	0.0
2	05 - 08	3.4 - 3.6	1.7 - 1.85	06.7±0.7	3.493±0.043	6.395±0.100	05.9
3	@	3.8 - 4.0	1.68 - 1.8	23.7±1.1	3.871±0.029	6.517±0.051	12.6
4	55 - 70	4.3 - 4.7	1.68 - 1.8	62.5±2.1	4.548±0.012	7.650±0.022	36.3
5	55 - 70	4.3 - 4.7	1.68 - 1.8	65.1±0.9	4.588±0.019	7.726±0.038	98.8
6	20 - 40	4.3 - 4.7	1.68 - 1.8	35.2±2.4	4.676±0.021	7.912±0.068	163.9
7	28 - 48	4.3 - 4.7	1.68 - 1.8	41.6±3.8	4.528±0.058	7.642±0.111	199.1
8	50 - 70	4.3 - 4.7	1.68 - 1.8	59.8±3.0	4.434±0.041	7.494±0.085	240.7
9	50 - 70	4.3 - 4.7	1.68 - 1.8	62.4±2.6	4.383±0.054	7.404±0.101	300.5
10	10 - 30	4.3 - 4.7	1.68 - 1.8	18.0±4.9	4.632±0.051	7.868±0.119	362.9
11	$	4.7	1.732	19.1	4.70	8.60	380.9
12	∞	5.08	1.842	∞	5.08	9.10	400.0

Table 5. The search range of the 12-layered model and the accepted structure. V_P: *P*-wave velocity; V_S: S-wave velocity. Values after '±' show the corresponding standard deviations. @: Thickness of 3rd layer = Crustal thickness - Sum of thickness of top two layers. Search range of crustal thickness 35-40 km. Crustal thickness of the accepted structure is 36.3 km. $: Thickness of 11th layer = (400 - sum of the thickness of top ten layers) km; Depth of LAB = Top of 7th layer = 199.1 ± 9.6 km.

8.4 Velocity structure of northern India

S.S RAI and D.S RAMESH summarized the work Indian researchers during the time of 2008-11 in the domain of structural seismology in the domain of structural seismology which deals with processes responsible for generation and evolution of the continent, and its linkage with the earthquake genesis. According to their study Garhwal Himalaya have nearly horizontal Moho at 35-40 km depth under the Lower Himalaya which suddenly steepens to a dip of 15-27° beneath the Higher Himalaya.

Another study done by Keith Priestle et al. (2007) on the basis of receiver function. They inverted the data of receiver function and surface wave dispersion. Thickness of the crust under the NDI is~40km. Crust thickness increases in foot hills to 50km and become more thick upto 60-65km, below the highest part of Himalaya. From south of the Indus Zangpo Suture (IZS) to the Karakorum Fault, the Moho deepens from 70 to 75 km below the surface.

8.5. surf96

The program enhance the visualization of the results. The following steps give an interactive step to proceed for the inversion of dispersion data.

Interactive control file setup

The following example shows the interactive dialog for the case that the dispersion file is named as JOINT_DISP and initial earth model file is in MODEL.txt

Determination of surface wave dispersion requires a search in the frequency – phase velocity space of the surface-wave period equation. It is known that all surface wave modes are bounded at the low end by some fraction of the smallest shear-wave velocity, or in the case of a surface fluid layer, the lowest compressional-wave velocity. The upper bound of the dispersion for a fixed period, is the half-space shear-wave velocity. dcl and dcr are the search increments to find the roots of the period equation. If these numbers are too large, modes may be missed by jumping past them. If the numbers are too small, computations take too long. The value of 0.005 km/sec are acceptable for crustal studies, but could be made smaller when studying dispersion in low velocity sediments.

parameter h is used to compute group-velocity partial derivatives. For example, $\partial U/\partial Vs$ can be computed by using $\partial c/\partial V(f)s$ and $\partial U/\partial V(1+h)fs$. The recommended value of 0.005 seems adequate.

The further process is been directed by the options available.

If all the model data and dispersion values has been input correctly, then a menu is displayed with a number of functions.

The next step is to go to option 32 to enter the damping values obtained earlier. Further control over the operation has been learnt from manual for surf96 by Herrmann, 2002.

CHAPTERS#9 RESULTS

9.1. Dispersion curves

Since the mode of propagation for Rayleigh waves is ellipsoidal, its dispersion is observed in only Radial and vertical component of the seismogram. The dispersion curves of Love waves is obtained from Transverse component of the seismogram. It's evident from the dispersion value that group velocity of Love waves is greater than Rayleigh waves.

Various dispersion curves are obtained from at BHOPAL station.

Love and Rayleigh waves for cluster 1

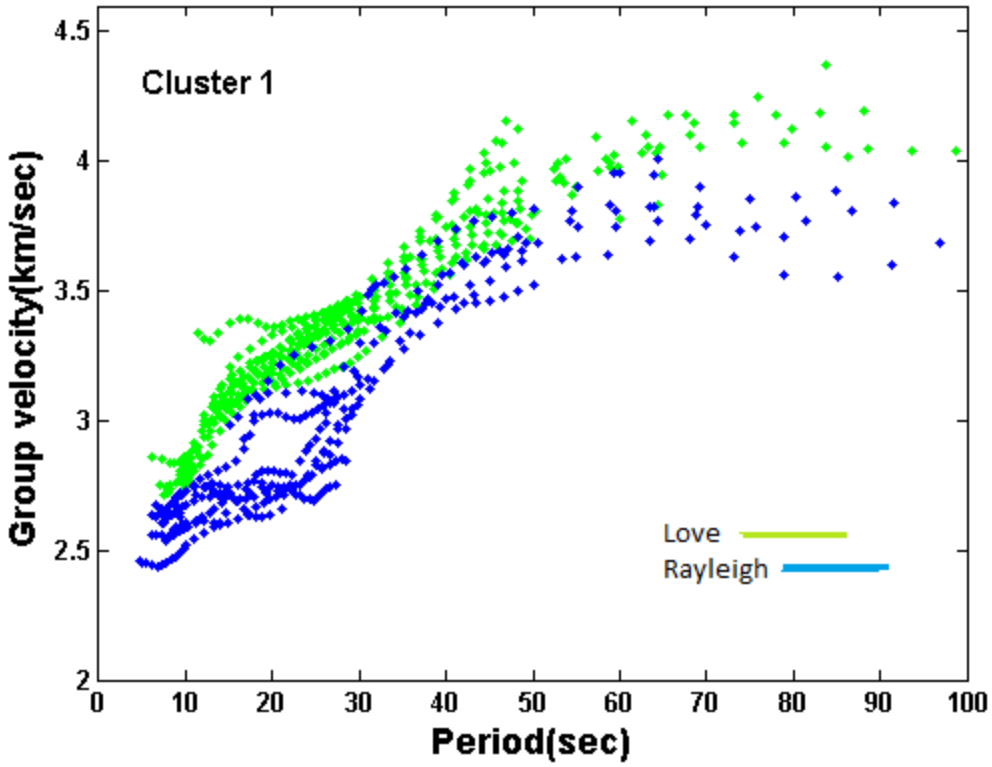

Figure 9.1. Love and Rayleigh dispersion curves for Bhopal station for **cluster 1** obtained by Multiple Filter Technique.

The curves shown in Figure 9.1. with green lines are love waves and those with blue lines are Rayleigh waves. The fig shows a simultaneous plot of both the curves. It's clearly seen from the plot that group velocity of love waves is always greater than those of Rayleigh waves. In lower periods (10-50s) the difference is less but as we move to higher periods or lesser frequencies the velocity gap increases. The gap is distinct in period of 70-100s.

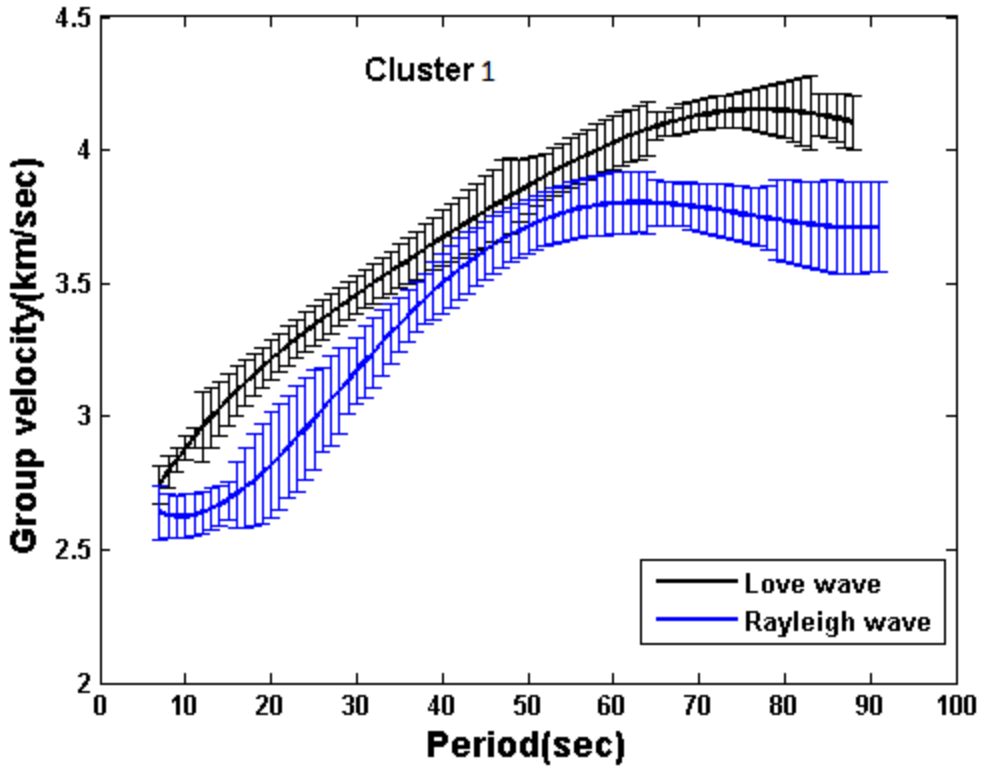

Figure 9.2. Love and Rayleigh weighted average dispersion curves for **cluster 1** obtained by polynomial fit to the weighted average

The polynomial fit to the weighted average plot shown in Figure 9.2 for the dispersion values for both Love and Rayleigh wave shows the distinctly the difference in velocities of the two type of waves.

Love and Rayleigh waves dispersion curves obtained from cluster 2

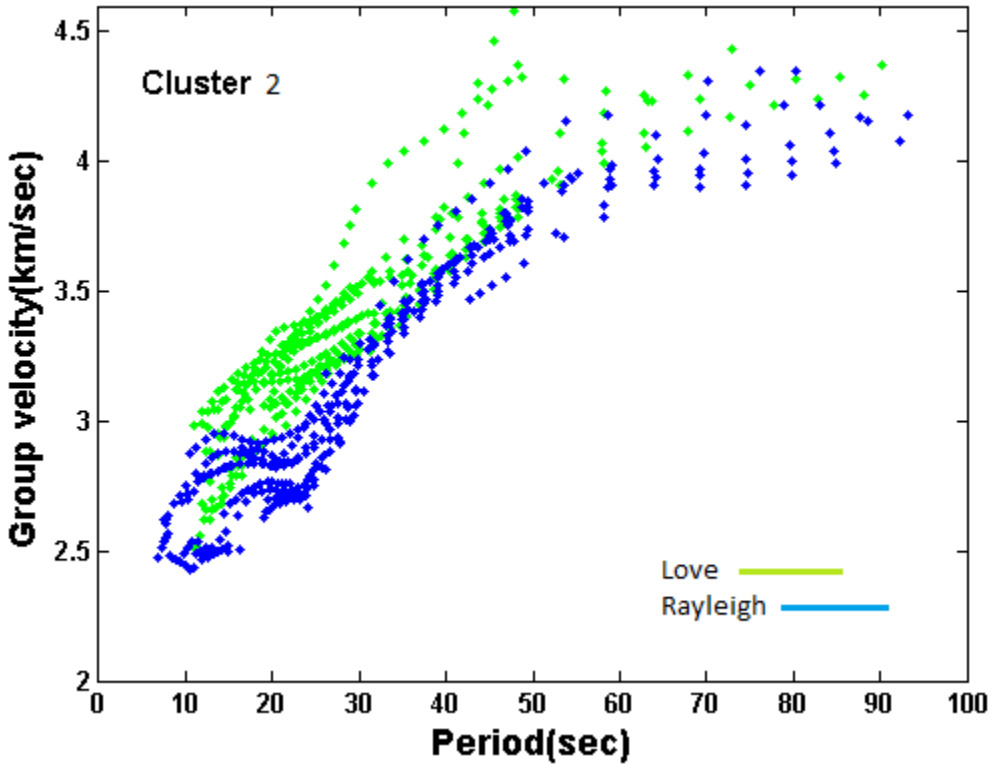

Figure 9.3. Love and Rayleigh dispersion curves for **cluster 2** obtained by Multiple Filter Technique.

The Figure 9.3 shows the variation of Love and Rayleigh waves group velocity obtained from cluster 2. These group velocities are obtained from events which are north-west of the station. The values of Love and Rayleigh waves are do not differ much in this cluster but still love wave have higher values.

To further analyze the scenario we obtained the polynomial fit to the weighted average of group velocity to see the difference distinctly.

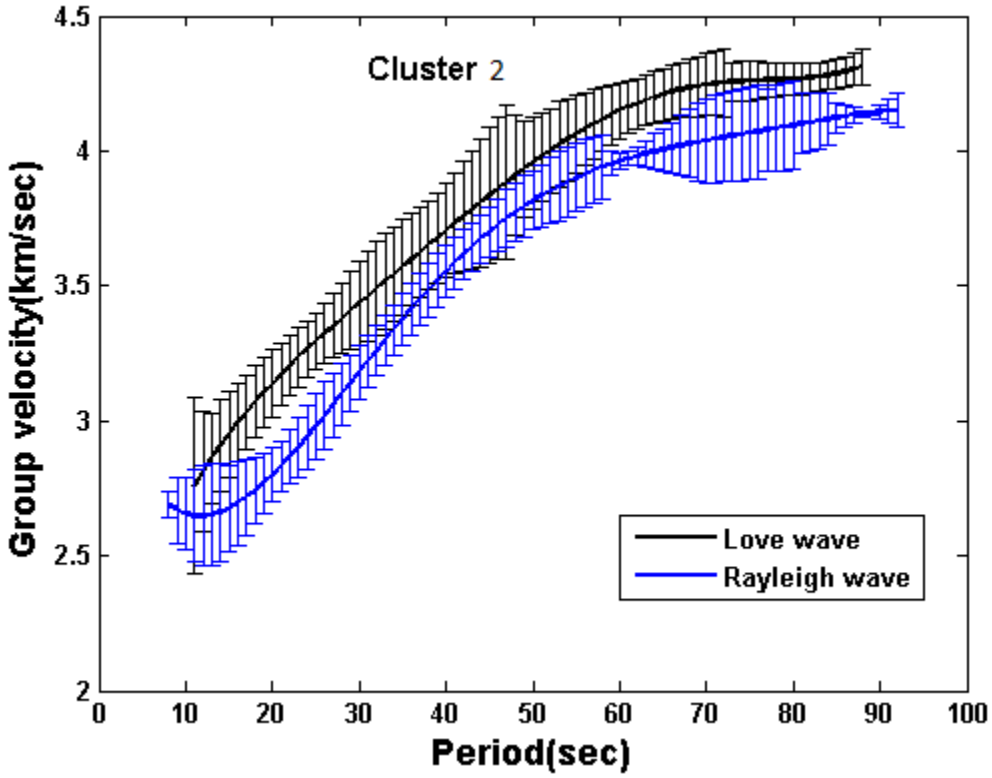

Figure 9.4. Love and Rayleigh weighted average dispersion curves for **cluster 2** obtained by polynomial fit to the weighted average.

From figure 9.4 same can be seen clearly seen as we see in figure 9.3 that the values of Love and Rayleigh waves are do not differ much in this cluster but still love wave have higher values.
So in this direction love wave and Rayleigh wave velocity don't have much difference as we have seen for the cluster 1. In this direction values of love and Rayleigh both exceed 4km/sec as compared to cluster 1 in which only love values exceed more than 4km/sec.

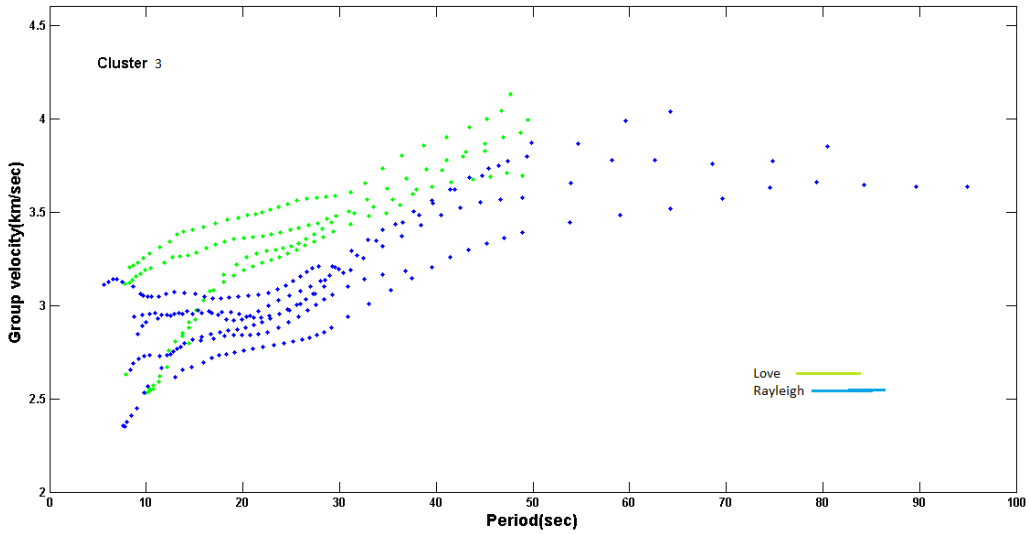

Figure 9.5. Love and Rayleigh dispersion curves for **cluster 3** obtained by Multiple Filter Technique.

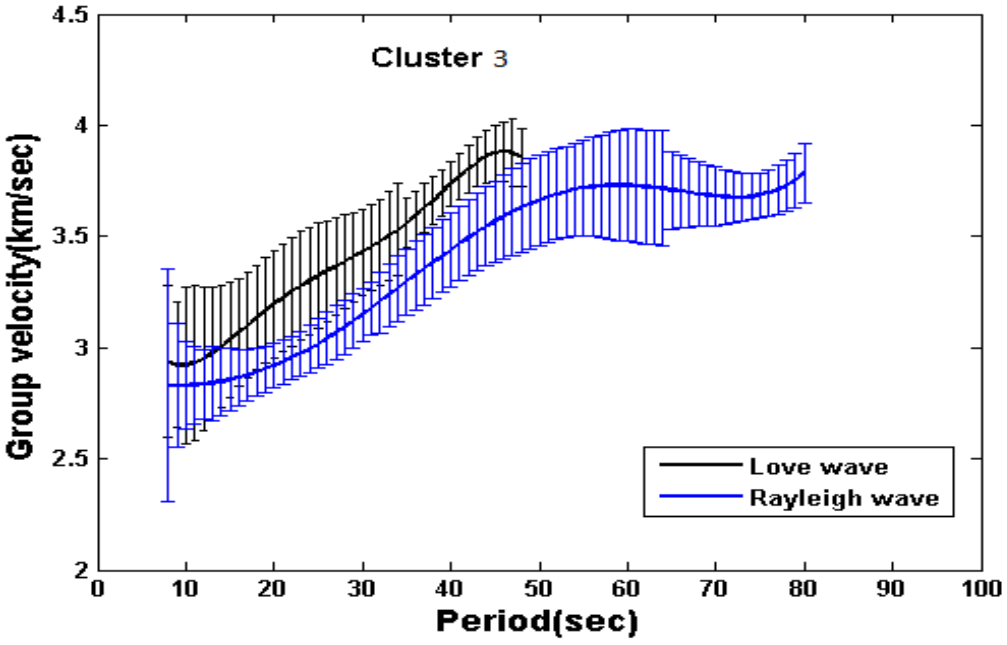

Figure 9.6. Love and Rayleigh weighted average dispersion curves for **cluster 3** obtained by polynomial fit to the weighted average.

From above figure 9.5 and 9.6 we can see that there is slight difference in values of love and Rayleigh wave, love wave having slightly higher values from period 10-50 sec. After 50 sec love

wave terminates but Rayleigh wave continues up to 85sec but did not exceed the values of love wave.

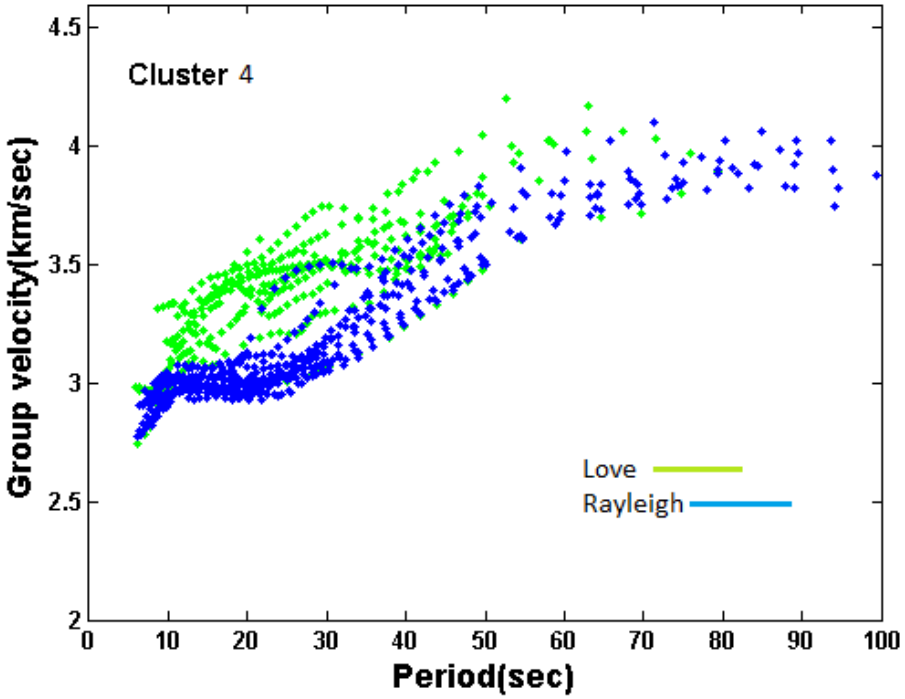

Figure 9.7. Love and Rayleigh dispersion curves for **cluster 4** obtained by Multiple Filter Technique.

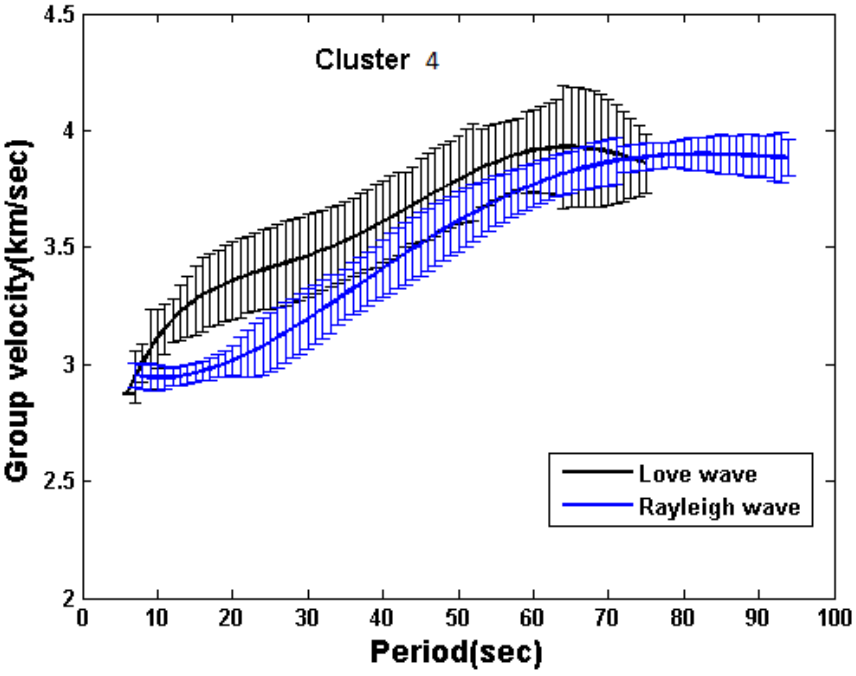

Figure 9.8. Love and Rayleigh weighted average dispersion curves for **cluster 4** obtained by polynomial fit to the weighted average.

On the basis of figure 9.7 and 9.8 for cluster 4 which is in just slightly west of north direction from Bhopal station have higher love wave values from period 10- 70 sec. but after 70 sec love wave terminates and Rayleigh continues up to approx. 95 sec. Cluster 4 shows almost same behavior like cluster 3 but in this cluster love values terminate at 70 sec as compared to cluster 3 which show love values termination at 50sec.

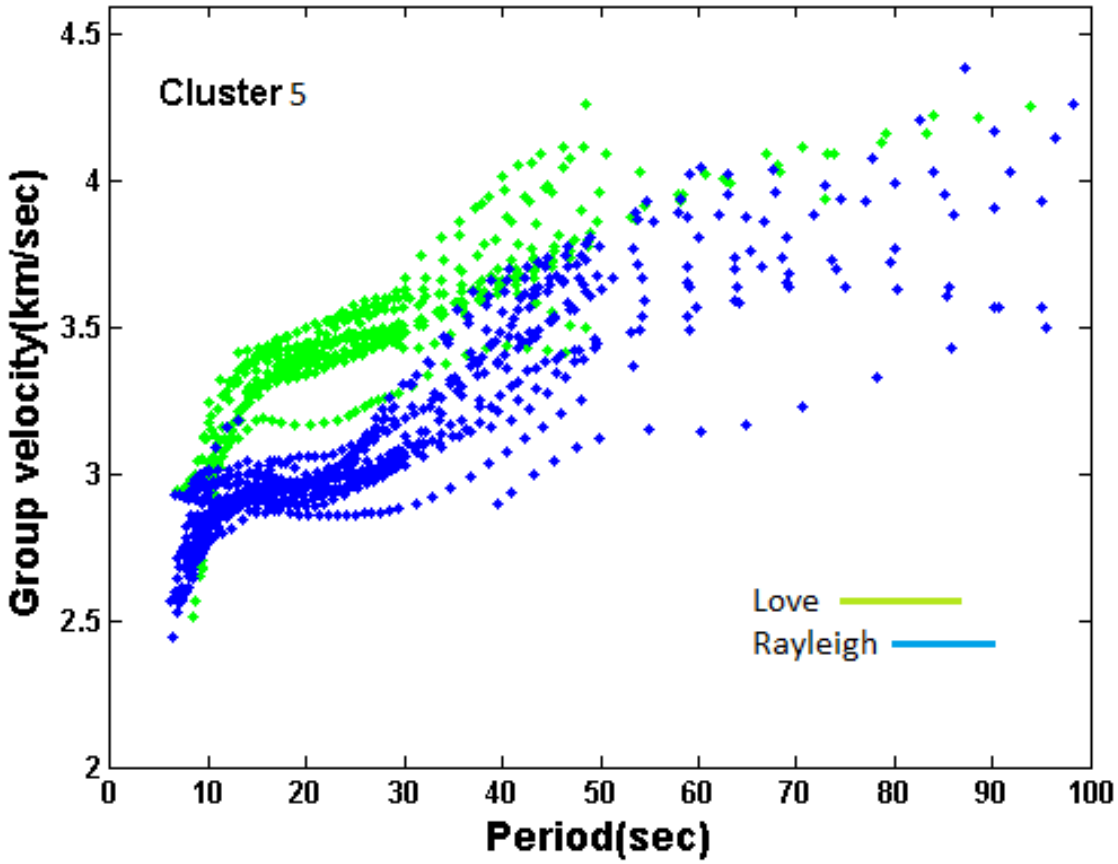

Figure 9.9. Love and Rayleigh dispersion curves for **cluster 5** obtained by Multiple Filter Technique.

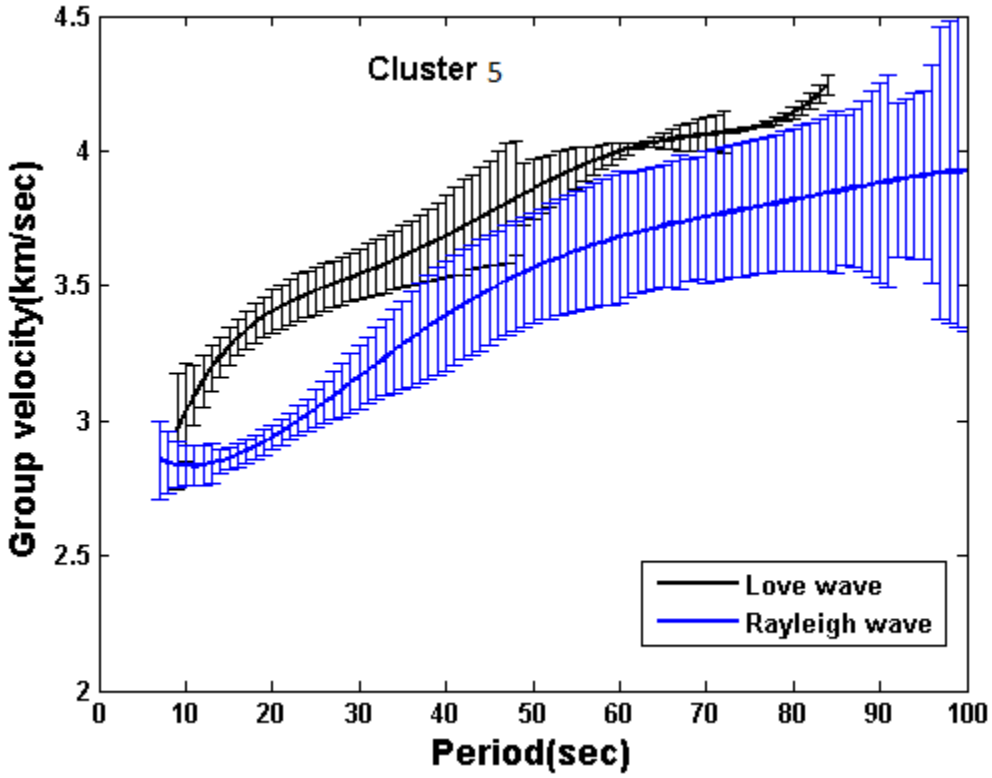

Figure 9.10. Love and Rayleigh weighted average dispersion curves for **cluster 5** obtained by polynomial fit to the weighted average.

From figure 9.9 and 9.10 for cluster 5 we can say that love values are higher than Rayleigh values from 10-85 sec. and in this love wave values continues up to 85 sec as compared to cluster 3 and 4 in which love values terminate earlier.

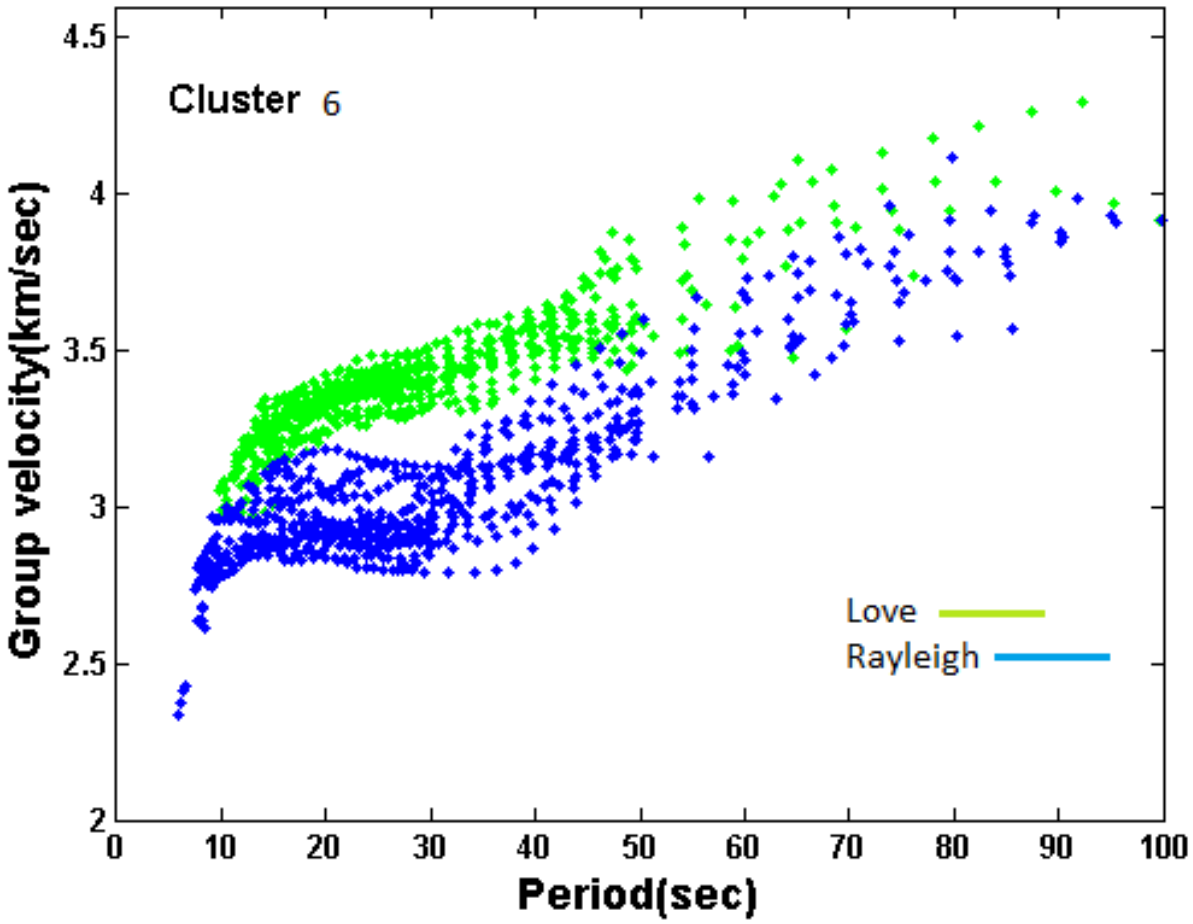

Figure 9.11 Love and Rayleigh dispersion curves for **cluster 6** obtained by Multiple Filter Technique.

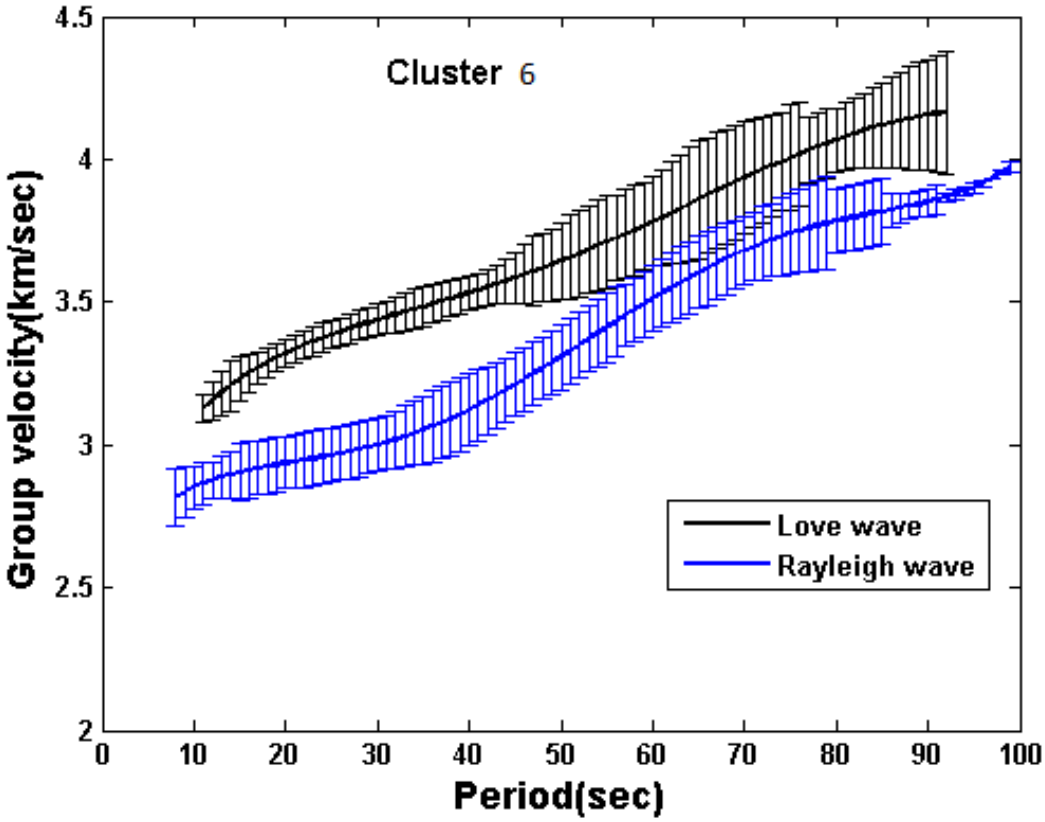

Figure 9.12. Love and Rayleigh weighted average dispersion curves for **cluster 6** obtained by polynomial fit to the weighted average.

Figure 9.11 and 9.12 for cluster 6 which is in north-east direction of the station Bhopal clearly show significant higher values of love than Rayleigh for period 10-55sec after 55 seconds the difference becomes low. Love wave do not terminate even after 85 sec.

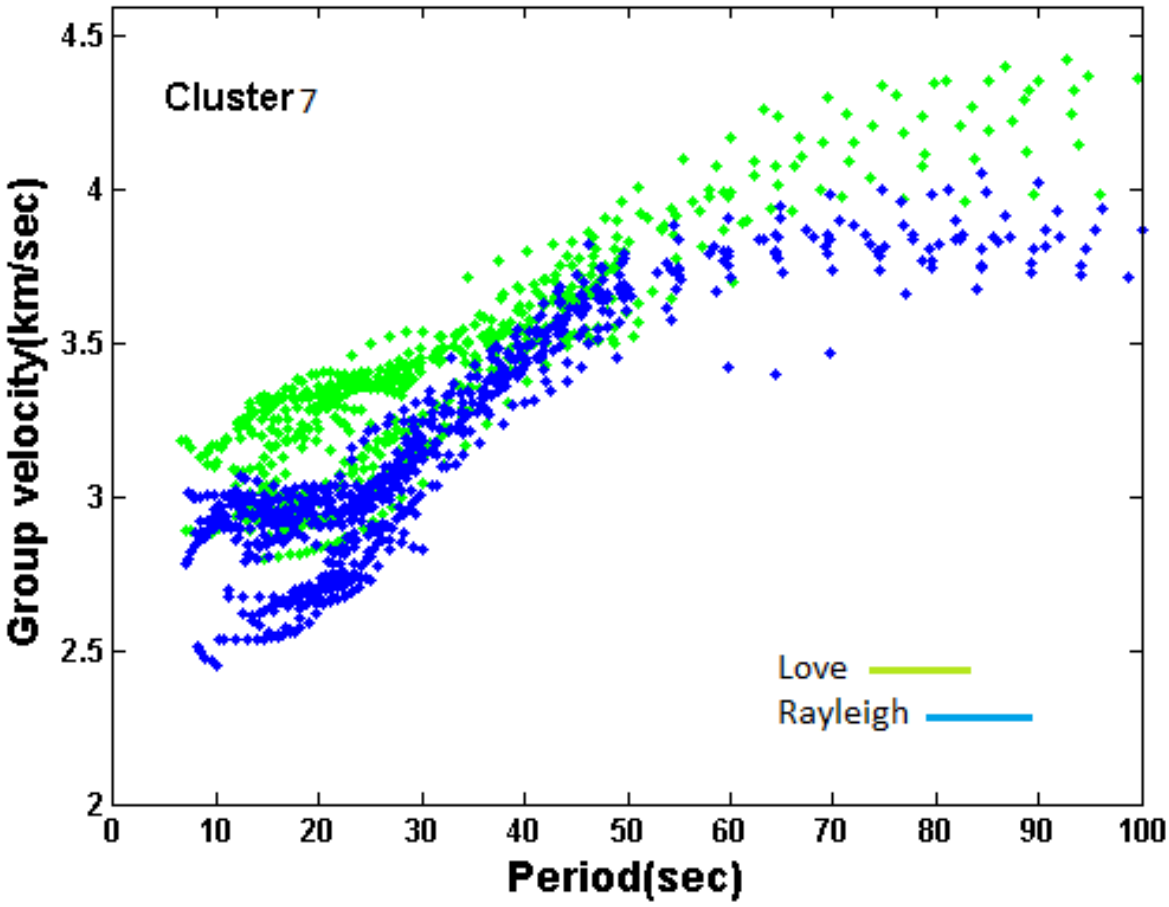

Figure 9.13 Love and Rayleigh dispersion curves for **cluster 7** obtained by Multiple Filter Technique.

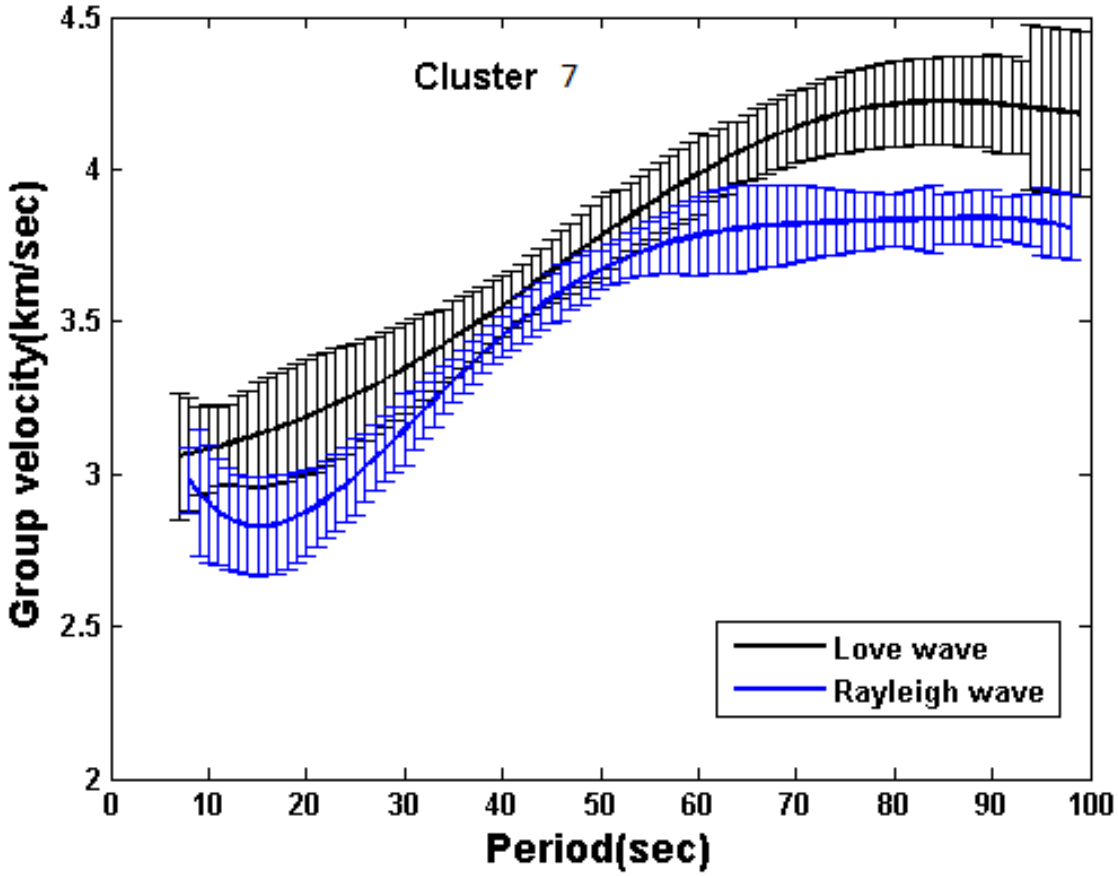

Figure 9.14 Love and Rayleigh weighted average dispersion curves for **cluster 7** obtained by polynomial fit to the weighted average.

From figure 9.13 and 9.14 for cluster 7 which is in east direction of the Bhopal station, we can clearly state that love values are higher than Rayleigh for first 10-30sec than the difference become less at 35- 55 second range again the difference become higher at 70-90 seconds period. In this cluster both waves continues even after 90 seconds of period.

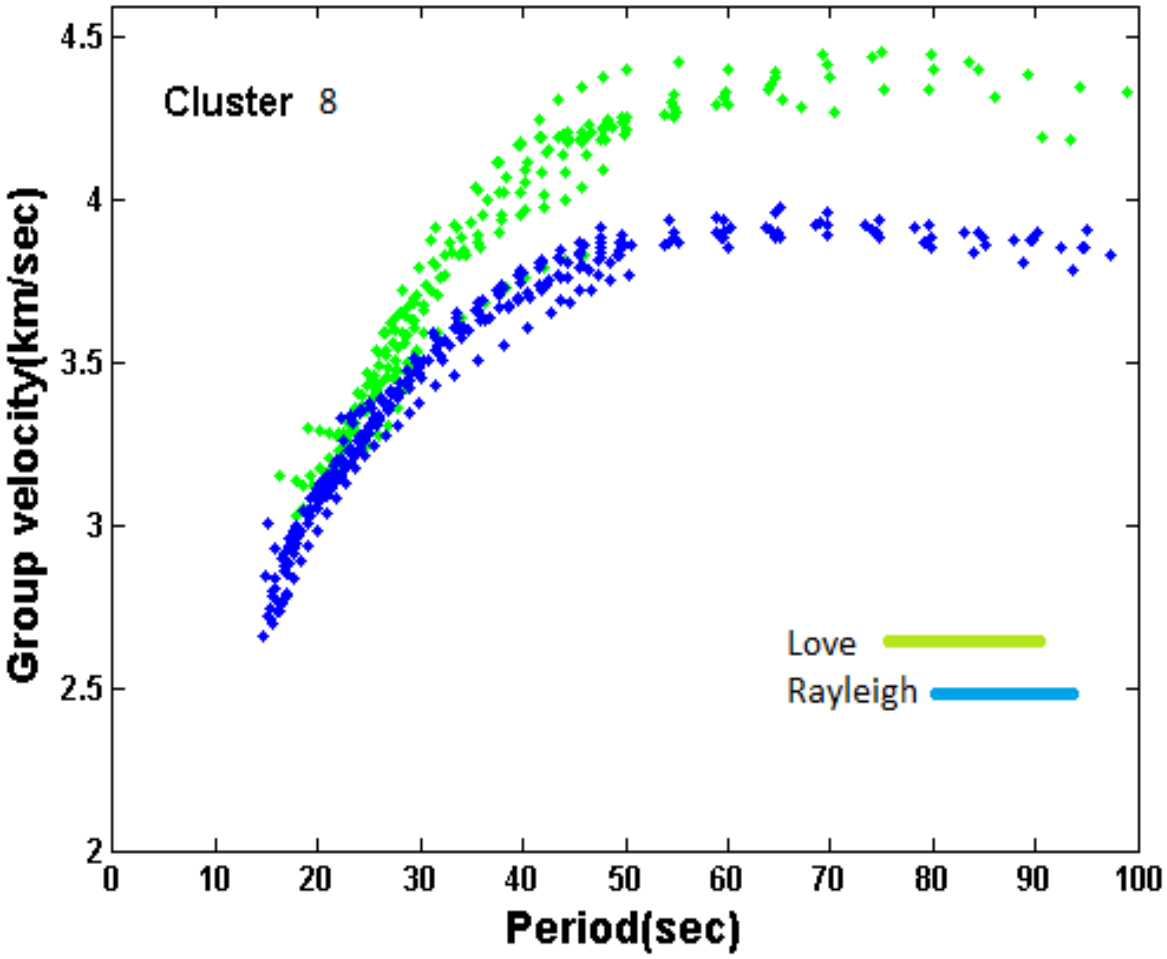

Figure 9.15 Love and Rayleigh dispersion curves for **cluster 8** obtained by Multiple Filter Technique.

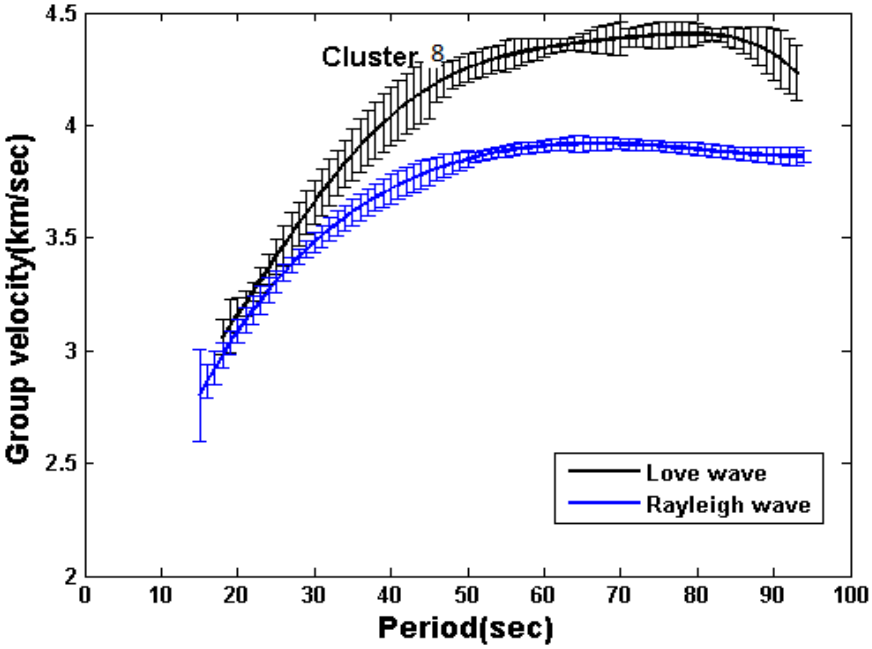

Figure 9.16 Love and Rayleigh dispersion curves for **cluster 8** obtained by Multiple Filter Technique.

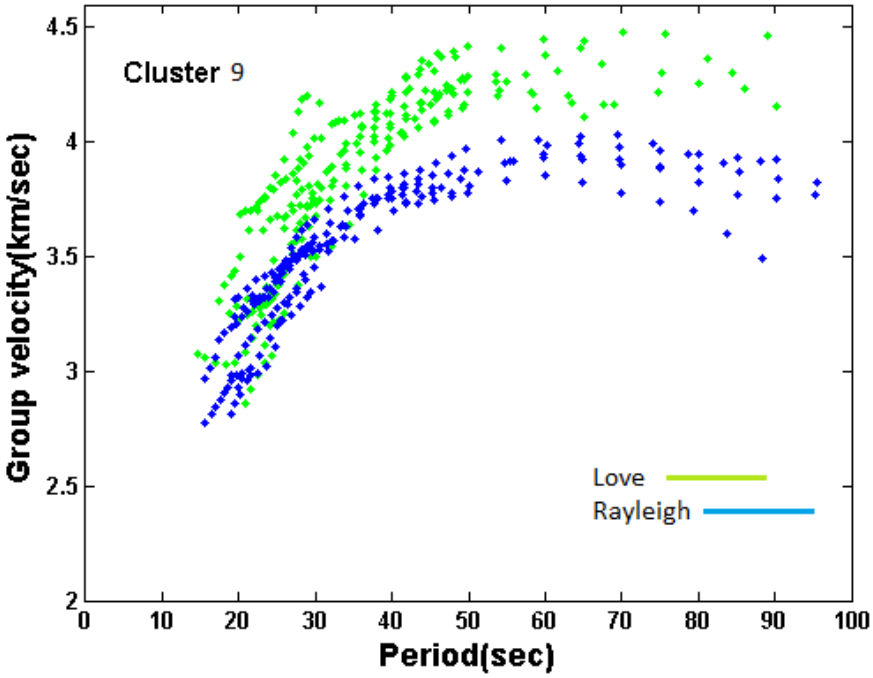

.

Figure 9.17 Love and Rayleigh dispersion curves for **cluster 9** obtained by Multiple Filter Technique.

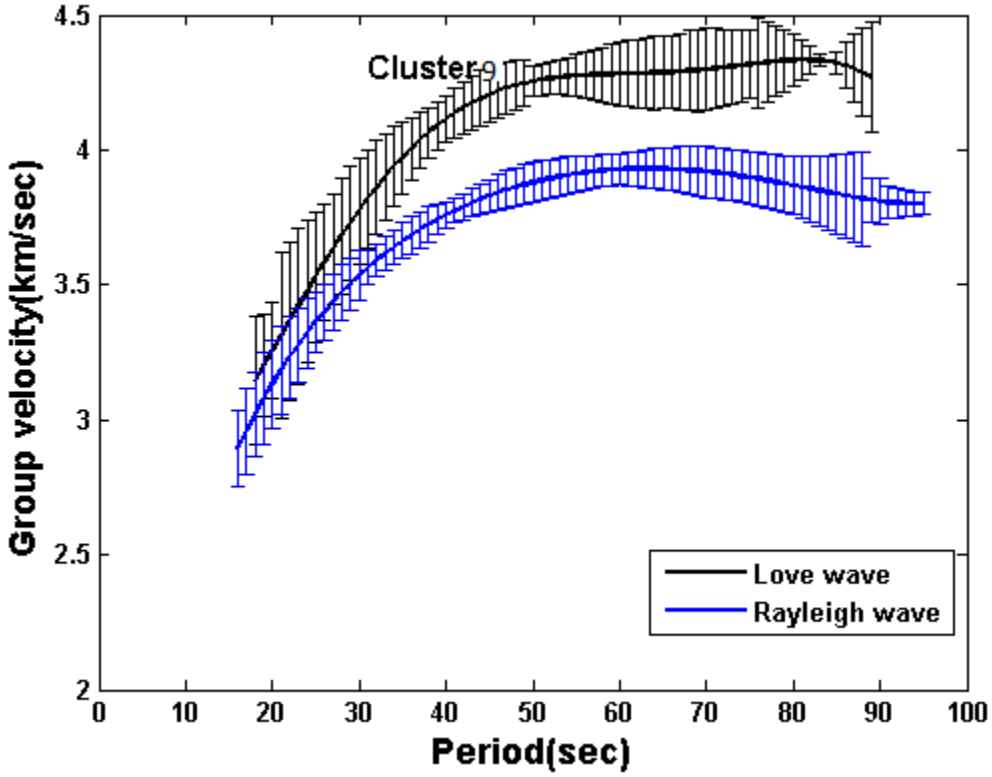

Figure 9.18 Love and Rayleigh dispersion curves for **cluster 9** obtained by Multiple Filter Technique.

Figure 9.15 and 9.16 which for cluster 8 and fig. 9.17 and 9.18 for cluster 9 which are in south-east direction of the station Bhopal. In these clusters events are coming from bay of Bengal.

Both cluster are showing same kind of behavior yet significantly different from other cluster as events in cluster 8 and 9 are coming from oceanic crust and in other clusters events were from continental crust.

So from last 4 figures we can clearly see that love and Rayleigh values were slightly different for 10-35 second period but after 35 sec. the difference become significantly high. In these 2 cluster love wave show higher values reaching almost 4.5km/sec.

9.2. Inversion result

After conducting inversion for 5 different cluster in different direction with initial model having 200 layers each of thickness 1km and using the dispersion curves obtained at Bhopal station the following output models is observed.

Output models

For cluster 1

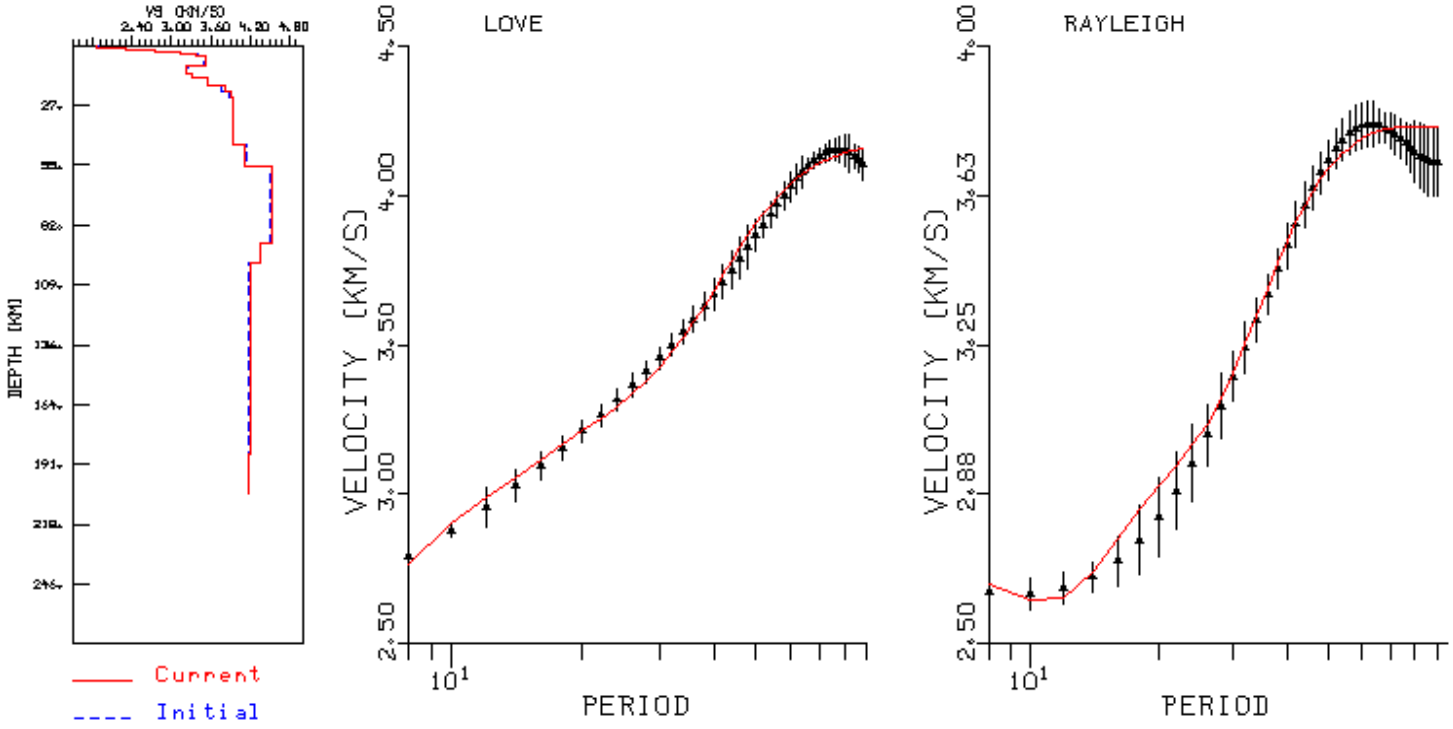

Figure 9.19 The output model for cluster 1 which is in west of the Bhopal station.

Table 9.1. The output model for cluster 1 which is in west of the Bhopal station.

layers(N)	H(KM)	VP(KM/S)	VS(KM/S)	RHO(GM/CC)	QP	QS
1	1	3.2365	1.8686	2.1878	5.00E-03	1.00E-02
2	1	3.9894	2.3035	2.318	5.00E-03	1.00E-02
3	1	4.7778	2.7595	2.4511	5.00E-03	1.00E-02
4	1	5.4206	3.1292	2.5843	5.00E-03	1.00E-02
5	1	5.8648	3.3868	2.6731	5.00E-03	1.00E-02
6	4	6.0839	3.5128	2.725	5.00E-03	1.00E-02
7	4	5.5941	3.2292	2.6189	5.00E-03	1.00E-02
8	2	5.7185	3.3022	2.6438	5.00E-03	1.00E-02
9	3	6.1515	3.5525	2.7454	5.00E-03	1.00E-02
10	3	6.591	3.8055	2.8734	5.00E-03	1.00E-02
11	3	6.7929	3.9213	2.926	5.00E-03	1.00E-02
12	21	6.8196	3.9325	2.9331	5.00E-03	1.00E-02
13	10	7.1568	4.1336	3.0301	5.00E-03	1.00E-02
14	35	7.8333	4.5244	3.2532	5.00E-03	1.00E-02
15	9	7.5433	4.3554	3.155	5.00E-03	1.00E-02
16	87	7.2767	4.2035	3.0685	5.00E-03	1.00E-02
17	0	7.2564	4.1913	3.062	1.11E-03	2.00E-03

Cluster 4 output model

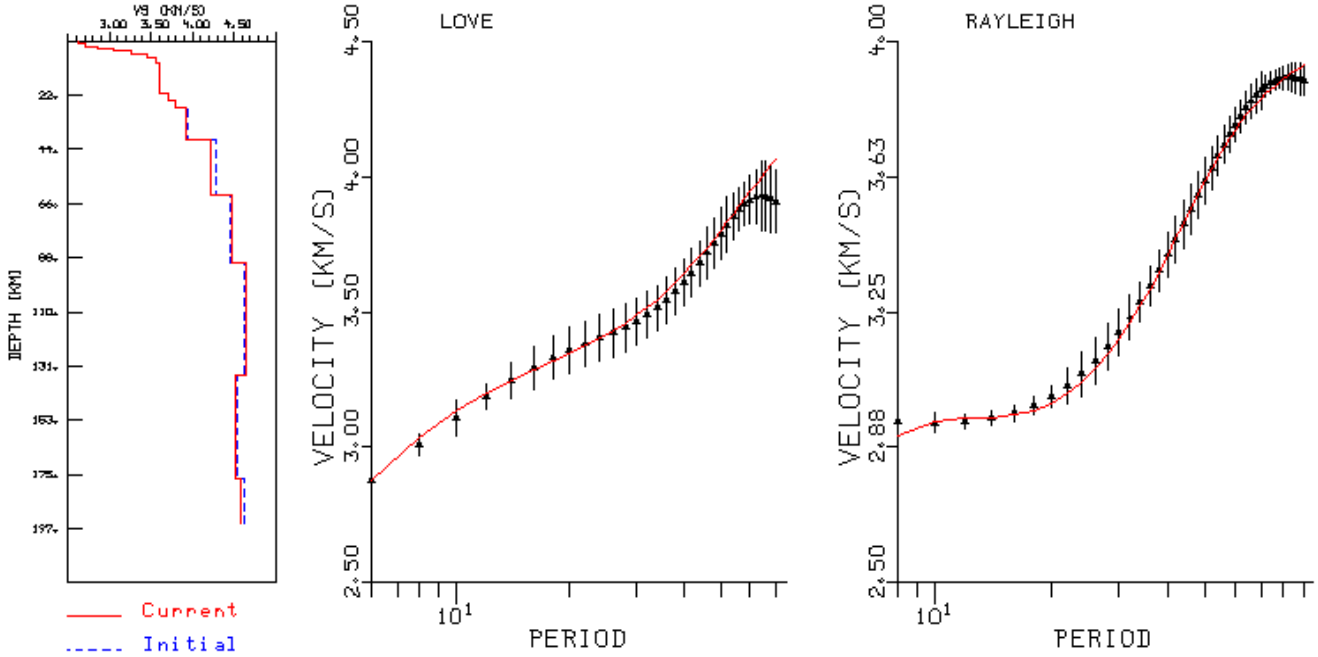

Figure 9.20 The output model for cluster 4 which is in slightly west of north of the Bhopal station.

Table 9.2 The output model for cluster 4 which is in slightly west of north of the Bhopal station.

layers(N)	H(KM)	VP(KM/S)	VS(KM/S)	RHO(GM/CC)	QP	QS
1	1	4.5557	2.6271	2.4023	5.00E-03	1.00E-02
2	1	4.6851	2.7096	2.4307	5.00E-03	1.00E-02
3	1	4.9299	2.8572	2.4846	5.00E-03	1.00E-02
4	1	5.2842	3.053	2.5568	5.00E-03	1.00E-02
5	1	5.6485	3.2582	2.6297	5.00E-03	1.00E-02
6	2	5.992	3.4605	2.6984	5.00E-03	1.00E-02
7	2	6.1726	3.5609	2.7517	5.00E-03	1.00E-02
8	12	6.2239	3.5994	2.7672	5.00E-03	1.00E-02
9	3	6.4419	3.7168	2.8325	5.00E-03	1.00E-02
10	3	6.5717	3.8037	2.8686	5.00E-03	1.00E-02
11	13	6.8124	3.9313	2.9312	5.00E-03	1.00E-02
12	22	7.3167	4.2274	3.0814	5.00E-03	1.00E-02
13	28	7.7639	4.4701	3.2297	5.00E-03	1.00E-02
14	45	8.0704	4.6476	3.3353	5.00E-03	1.00E-02
15	42	7.8054	4.5129	3.2439	5.00E-03	1.00E-02
16	0	7.9587	4.5884	3.296	1.11E-03	2.00E-03

Cluster 6 output model

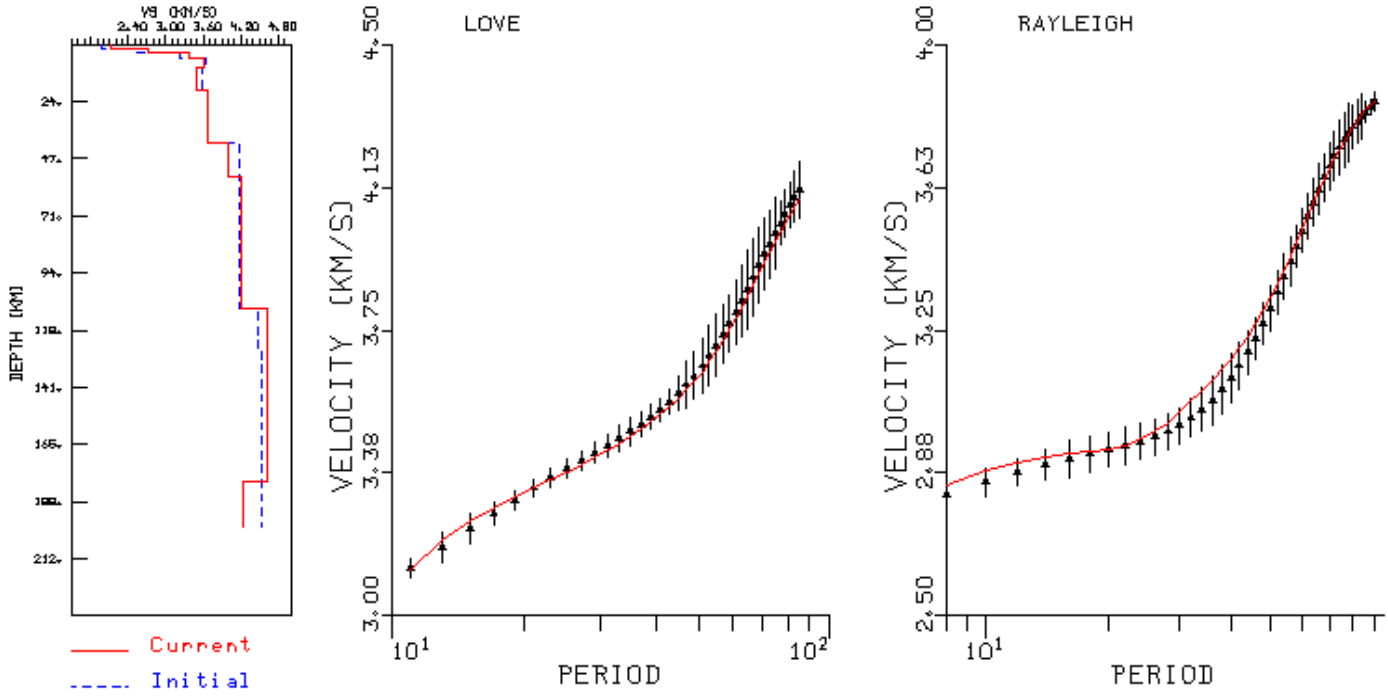

Figure 9.21 The output model for cluster 6 which is in north-east of the Bhopal station.

Table 9.3 The output model for cluster 6 which is in north-east of the Bhopal station

layers(N)	H(KM)	VP(KM/S)	VS(KM/S)	RHO(GM/CC)	QP	QS
1	1.5	3.6948	2.1283	2.27E+00	5.00E-03	1.00E-02
2	2	4.7146	2.7173	2.44E+00	5.00E-03	1.00E-02
3	2	5.8655	3.3873	2.67E+00	5.00E-03	1.00E-02
4	4	6.2649	3.6124	2.78E+00	5.00E-03	1.00E-02
5	9	6.0625	3.5048	2.72E+00	5.00E-03	1.00E-02
6	22	6.3795	3.6797	2.81E+00	5.00E-03	1.00E-02
7	14	6.9213	3.9976	2.96E+00	5.00E-03	1.00E-02
8	54	7.2728	4.2008	3.07E+00	5.00E-03	1.00E-02
9	17	8.0429	4.6389	3.33E+00	5.00E-03	1.00E-02
10	55	8.0186	4.6255	3.32E+00	5.00E-03	1.00E-02
11	0	7.3541	4.2424	3.11E+00	1.11E-03	2.00E-03

Cluster 7 output model

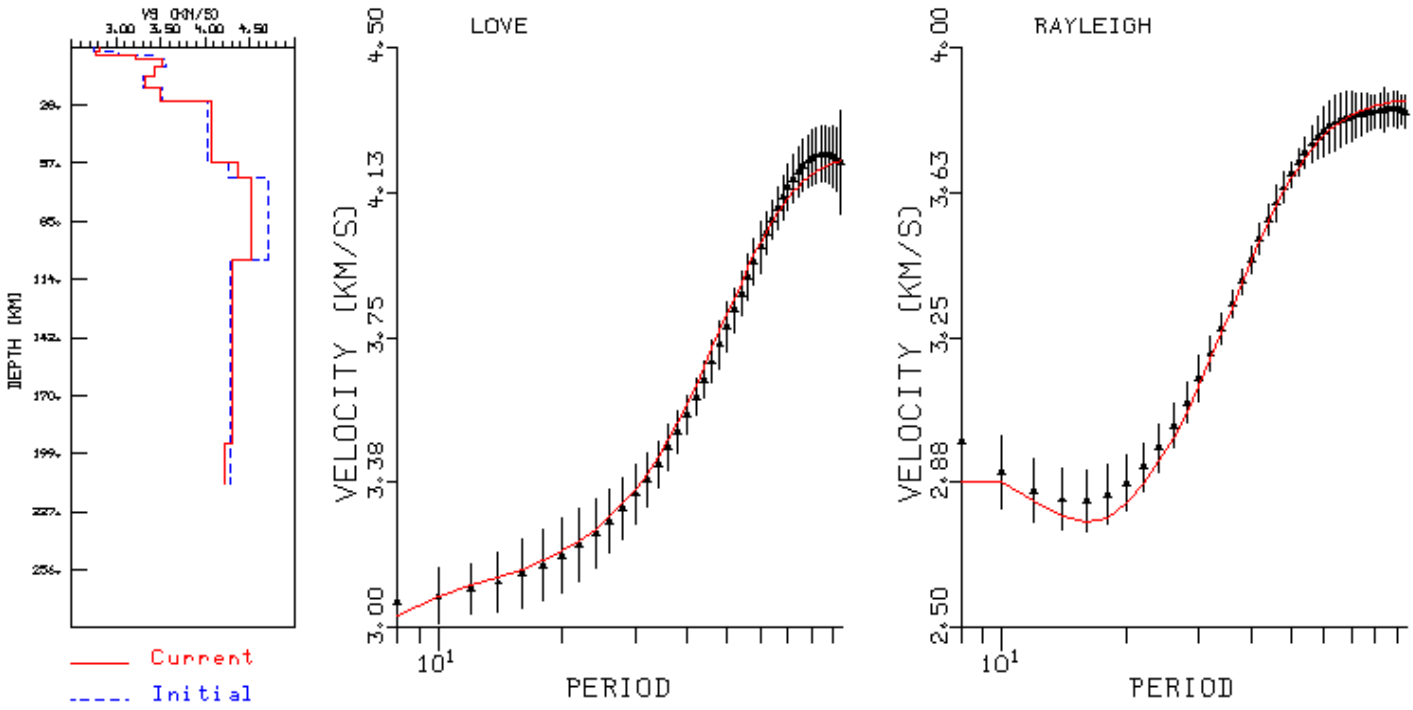

Figure 9.22 The output model for cluster 6 which is in east of the Bhopal station.

Table 9.4 The output model for cluster 7 which is in east of the Bhopal station.

layers(N)	H(KM)	VP(KM/S)	VS(KM/S)	RHO(GM/CC)	QP	QS
1	2	4.8968	2.8277	2.48E+00	5.00E-03	1.00E-02
2	2	4.8086	2.7749	2.46E+00	5.00E-03	1.00E-02
3	2	5.5898	3.227	2.62E+00	5.00E-03	1.00E-02
4	4	6.0896	3.5173	2.73E+00	5.00E-03	1.00E-02
5	4	5.9329	3.4244	2.69E+00	5.00E-03	1.00E-02
6	6	5.7622	3.3282	2.65E+00	5.00E-03	1.00E-02
7	6	6.046	3.4925	2.71E+00	5.00E-03	1.00E-02
8	30	7.0539	4.0725	3.00E+00	5.00E-03	1.00E-02
9	8	7.5626	4.3664	3.16E+00	5.00E-03	1.00E-02
10	40	7.8228	4.5176	3.25E+00	5.00E-03	1.00E-02
11	90	7.4787	4.3176	3.13E+00	5.00E-03	1.00E-02
12	0	7.3306	4.2321	3.08E+00	1.11E-03	2.00E-03

Output model for the Cluster 9

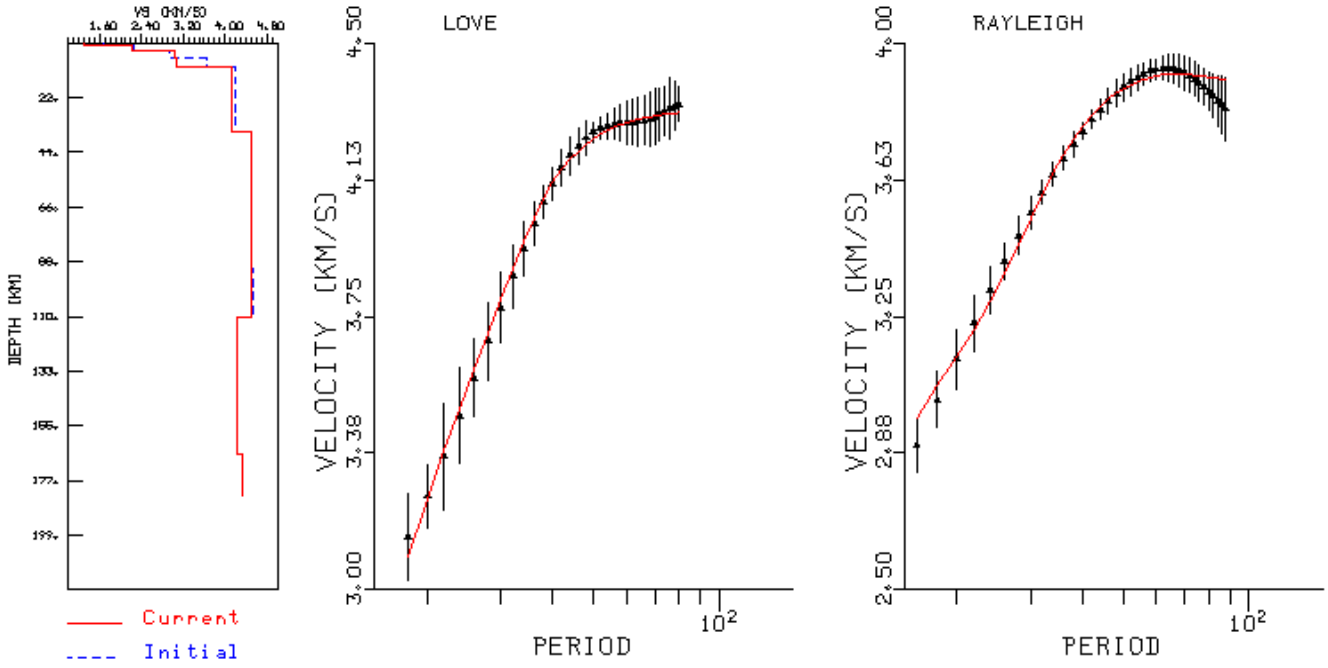

Figure 9.23 The output model for cluster 9 which is in south-east of the Bhopal station or in bay of Bengal.

Table 9.5 The output model for cluster 9 which is in in south-east of the Bhopal station or in bay of Bengal.

layers(N)	H(KM)	VP(KM/S)	VS(KM/S)	RHO(GM/CC)	QP	QS
1	1	2.2555	1.3023	2.39E+00	5.00E-03	1.00E-02
2	2	3.8323	2.2123	2.29E+00	5.00E-03	1.00E-02
3	3	5.2894	3.0553	2.56E+00	5.00E-03	1.00E-02
4	4	5.3235	3.0751	2.56E+00	5.00E-03	1.00E-02
5	26	7.179	4.1444	3.04E+00	5.00E-03	1.00E-02
6	55	7.8236	4.5169	3.25E+00	5.00E-03	1.00E-02
7	20	7.8207	4.5136	3.25E+00	5.00E-03	1.00E-02
8	55	7.3341	4.2348	3.09E+00	5.00E-03	1.00E-02
9	0	7.495	4.3264	3.14E+00	1.11E-03	2.00E-03

.

CHAPTER#9 CONCLUSION AND INTERPERTATION

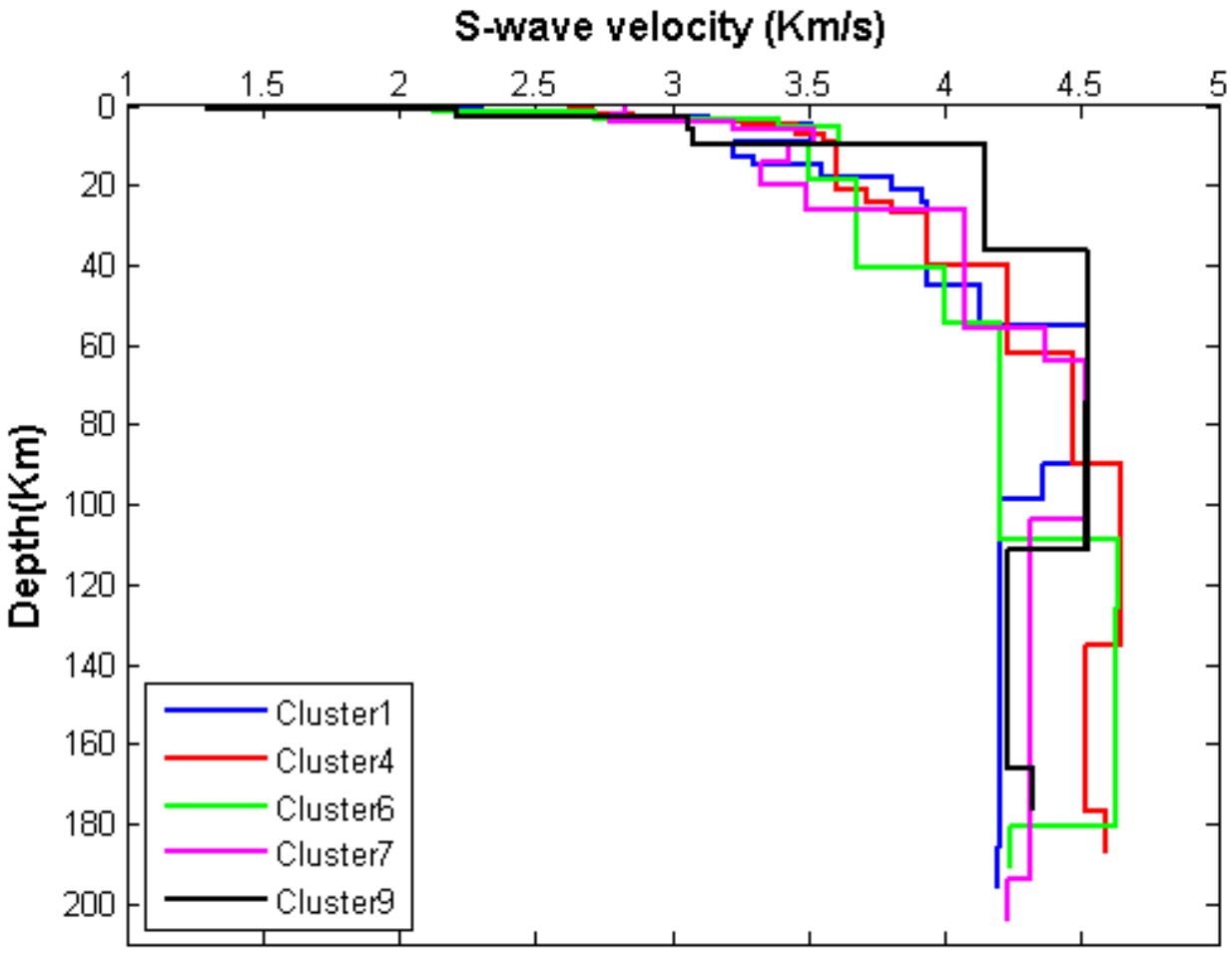

Figure 10.1 The final output S-wave velocity structure obtained for 5 different cluster for Bhopal station.

Cluster 1 is for the events in west direction of Bhopal station.

Cluster 4 is for the events in slightly west of north direction of Bhopal station.

Cluster 6 is for the events in north-east direction of Bhopal station.

Cluster 7 is for the events in east direction of Bhopal station.

Cluster 9 is for the events in south-east direction of Bhopal station.

1) The inversion result for cluster 1 shows 1 km thick upper layer with an average Vs of 1.86 km/s above a ~ 1 km thick layer of Vs 2.3 km/s. This is underlain by three layers of each ~1km thick with Vs of 2.7595 km/s, 3.1292 km/s and 3.3868km/s respectively. Below this is 4 km-thick layer with Vs of 3.5128 km/s. The Moho is at a depth of ~ 45 ± 3 km with a sub-Moho shear wave velocity of 3.9325 km/s.

2) The inversion result for cluster 4 shows top 5 layers of each 1 km thick with Vs of 2.62, 2.70, 2.85, 3.05, 3.25km/sec respectively with increasing depth followed by 2 layers of each 2 km thick having Vs 3.46 and 3.56 km/sec. Below this is 12 km thick layer with Vs of 3.59 km/s. The Moho is at a depth of ~ 59 ± 3 km with a sub-Moho shear wave velocity of 4.22 km/s.

3) The inversion result for cluster 6 shows top layer with 1.5km thick with an average Vs of 2.12 km/s above 2 layers each of 2 km thick with Vs of 2.71 and 3.38 km/s respectively with increasing depth. This is underlain by two layers of 4 km and 9 km with Vs of 3.61 and 3.50 km/s. The Moho is at a depth of ~ 54 ± 3 km with a sub-Moho shear wave velocity of 3.99 km/s.

4) The inversion result for cluster 7 shows top 3 layer with each 2 km thick having Vs of 2.82, 2.77 and 3.22 km/sec respectively with increasing depth followed by 2 layers of each 4 km thick having Vs 3.51 and 3.42 km/sec. The Moho is at a depth of ~ 56 ± 3 km with a sub-Moho shear wave velocity of 4.07 km/s.

5) The inversion result for cluster 9 shows top 3 layer with each 1, 2 and 3 km thick with Vs of 1.30. 2.21 and 3.05 km/s respectively. This is underlain by two layers of 4 and 26 km with Vs of 3.07 and 4.14 km /sec respectively. The Moho is at a depth of ~ 10 ± 3 km with a sub-Moho shear wave velocity of 4.14 km/s.

6) From figure 10.1 we can clearly see that velocity of S wave is highest for the cluster 9 as it is coming from the oceanic crust which have higher density and higher elastic moduli values than continental crust.

7) For cluster 9 moho is at depth of 10 ± 3 km and at this depth s wave velocity is 4.14km/sec which is highest among all the cluster at this depth. At this depth other cluster have Vs in range of 3.4-3.7km/sec.
8) We all know mountain have deep roots and deep crust but oceans have shallow moho because of isostatic equilibrium. Same can be inferred from above that moho is deepest 59 ± 3km at for the cluster 2 which is in region of hidhu-kush mountain region and shallowest for the cluster 9 which is in bay of Bengal region having oceanic crust.
9) Cluster no 7 also show deep moho at 56 ± 3 km which is also in mountainous region so it is also supporting the theory of isostasy.
10) Cluster 1, 9 and 7 show converging of Vs velocities at a depth of approx. 110 km showing a low velocity layer which is asthenosphere.

Reference

Bachman, R. T. & Hamilton, E. L., 1980. Sediment sound velocities from sonobuoys: Arabian Fan, J. geophys. Res., 85,849-852.

Brune, J., Singh, D., 1986. Continent-like crustal thickness beneath the Bay of Bengal sediments. Bull. Seismol. Soc. Am. 76, 191–203.

Chave, A. D., 1979. Lithospheric structure of the Walvis Ridge from Rayleigh wave dispersion, J. geophys. Res., 84,6840-6848.

Curray, J.R., F.J. Emmel, D.G. Moore, and W.R. Russel, 1982.Structure, tectonics, and geological history of the northeastern Indian ocean ,in The Ocean Basins and Margins, The Indian Ocean, vol. 6, edited by A.E. Naim and EG. Stheli, pp. 399-450, Plenum, New York.

Dziewonski, A., S. Bloch, and M. Landisman,1969: A technique for the analysis of transient seismic signals. Bull. Seismol. Soc. Am., 59, 427- 444.

Gabriel, V. G. & Kuo, J. T., 1966. High Rayleigh wave phase velocities for the New-Dehli, IndiaLahore, Pakistan profile, Bull. seism. Soc. Am., 56, 1137-1145.

Gaddale Suresh,, Sankar N. Bhattacharya, Satbir S. Teoti, Crust and upper mantle velocity structure of the northwestern Indian Peninsular Shield from inter-station phase velocities of Rayleigh and Love waves, ANNALS OF GEOPHYSICS, 58, 2, 2015.

Gopala Rao, D., K.S. Krishna, and D. Sar, 1997. Crustal evolution and sedimentation history of the Bay of Bengal, since the Cretaceous J,. Geophys, Res.,1 02, 17,747-17,76.

Herrmann, R. B., and Ammon, C. J., 2004. Computer programs in seismology version 3.20: Surface waves, receiver functions, and crustal structure, St. Louis University, Missouri. Available at http://mnw.eas.slu.edu/People/RBHerrmann.

Keith Priestley, James Jackson and Dan McKenzie, Lithospheric structure and deep earthquakes beneath India, the Himalaya and southern Tibet, Geophys. J. Int. (2008) 172, 345–362.

Landsman M. A., Dziewonski and Sato Y., 1969. Recent improvements in the analysis of surface waves observations. Geophys. J. R. Astr. Soc. 17, 369 – 403.

Lévêque, J. J., 1980. Regional upper mantle S-velocity models from phase velocities of great circle Rayleigh waves, Geophys. J. R. astr. Soc., 63,23-43.

Levshin, A.L., Yanovskaya, T.B., Lander, A.V., Bukchin B.G., Barmin M.P., Ratnikova L.I., Its E.N., 1989. Seismic Surface Waves in Laterally Inhomogeneous Earth. (Ed. V.I.Keilis-Borok), Kluwer Publ. House, Dordrecht/ Boston/ London. Russian Edition (Nauka), 1988.

N. Purnachandra Rao, T. Tsukuda, M. Kosuga, S. C. Bhatia1 and G. Suresh, Deep lower crustal earthquakes in central India: inferences from analysis of regional broadband data of the 1997 May 21, Jabalpur earthquake Geophys. J. Int. (2002) 148, 132–138.

Ottemöller, Voss and Havskov, 2014. SEISAN EARTHQUAKE ANALYSIS SOFTWARE FOR WINDOWS, SOLARIS, LINUX and MACOSX.

Savage B, Goldstein P, and Snoke A , SAC Manual and Tutorial.

S. N. BttATTACHARYA October 198l, OBSERVATION AND INVERSION OF SURFACE WAVE GROUP VELOCITIES ACROSS CENTRAL INDIA, Bulletin of the Seismological Society of America, Vol. 7l, No. 5, pp. 1489-1501.

Snieder R., Trampert J., 2003., Linear and Nonlinear Inverse Problems Geomatic Method for the Analysis of Data in the Earth Sciences Lecture Notes in Earth Sciences Volume 95, 2000, pp 93164.

Shearer P., 2009. Introduction to seismology, Cambridge University Press, United Kingdom 215 pp.

Supriyo Mitra, Keith Priestley, Anjan Kr Bhattacharyya and V. K. Gaur,(2005) Crustal structure and earthquake focal depths beneath northeastern India and southern Tibet, Geophys. J. Int. 160,227-248.

S S RAI and D S RAMESH, Seismic Imaging of the Indian Continental Lithosphere, Proc Indian natn Sci Acad 78 No. 3 September 2012 pp. 353-359.

Trampert, J.,1998. Global seismic tomography: the inverse problem and beyond, Inverse Problems, 14, 371-385.

Udias, A. (1999). Principles of Seismology. Cambridge University Press, United Kingdom.